

Article

Assessment of the COVID-19 Lockdown Effects on Spectral Aerosol Scattering and Absorption Properties in Athens, Greece

Dimitris G. Kaskaoutis ^{1,2,*} , Georgios Grivas ¹, Eleni Liakakou ¹, Nikos Kalivitis ², Giorgos Kouvarakis ², Iasonas Stavroulas ¹, Panayiotis Kalkavouras ¹, Pavlos Zarmas ², Umesh Chandra Dumka ³, Evangelos Gerasopoulos ¹ and Nikolaos Mihalopoulos ^{1,2,*} 

¹ Institute for Environmental Research and Sustainable Development, National Observatory of Athens, 15236 Athens, Greece; ggrivas@noa.gr (G.G.); liakakou@noa.gr (E.L.); i.stavroulas@noa.gr (I.S.); pkalkavouras@noa.gr (P.K.); egera@noa.gr (E.G.)

² Environmental Chemical Processes Laboratory, Department of Chemistry, University of Crete, 70013 Heraklion, Greece; nkalivitis@chemistry.uoc.gr (N.K.); gkouvarakis@uoc.gr (G.K.); pzarmas@gmail.com (P.Z.)

³ Aryabhatta Research Institute of Observational Sciences, Nainital 263001, India; dumka@aries.res.in

* Correspondence: dkask@noa.gr (D.G.K.); nmihalo@noa.gr (N.M.); Tel.: +30-2108109219 (D.G.K.); +30-2108109121 (N.M.)



Citation: Kaskaoutis, D.G.; Grivas, G.; Liakakou, E.; Kalivitis, N.; Kouvarakis, G.; Stavroulas, I.; Kalkavouras, P.; Zarmas, P.; Dumka, U.C.; Gerasopoulos, E.; et al. Assessment of the COVID-19 Lockdown Effects on Spectral Aerosol Scattering and Absorption Properties in Athens, Greece. *Atmosphere* **2021**, *12*, 231. <https://doi.org/10.3390/atmos12020231>

Academic Editor: Gunnar W. Schade
Received: 3 January 2021
Accepted: 3 February 2021
Published: 8 February 2021

Publisher's Note: MDPI stays neutral with regard to jurisdictional claims in published maps and institutional affiliations.



Copyright: © 2021 by the authors. Licensee MDPI, Basel, Switzerland. This article is an open access article distributed under the terms and conditions of the Creative Commons Attribution (CC BY) license (<https://creativecommons.org/licenses/by/4.0/>).

Abstract: COVID-19 is evolving into one of the worst pandemics in recent history, claiming a death toll of over 1.5 million as of December 2020. In an attempt to limit the expansion of the pandemic in its initial phase, nearly all countries imposed restriction measures, which resulted in an unprecedented reduction of air pollution. This study aims to assess the impact of the lockdown effects due to COVID-19 on in situ measured aerosol properties, namely spectral-scattering (b_{sca}) and absorption (b_{abs}) coefficients, black carbon (BC) concentrations, single-scattering albedo (SSA), scattering and absorption Ångström exponents (SAE, AAE) in Athens, Greece. Moreover, a comparison is performed with the regional background site of Finokalia, Crete, for a better assessment of the urban impact on observed differences. The study examines pre-lockdown (1–22 March 2020), lockdown (23 March–3 May 2020) and post-lockdown (4–31 May 2020) periods, while the aerosol properties are also compared with a 3–4 year preceding period (2016/2017–2019). Comparison of meteorological parameters in Athens, between the lockdown period and respective days in previous years, showed only marginal variation, which is not deemed sufficient in order to justify the notable changes in aerosol concentrations and optical properties. The largest reduction during the lockdown period was observed for b_{abs} compared to the pre-lockdown (−39%) and to the same period in previous years (−36%). This was intensified during the morning traffic hours (−60%), reflecting the large decrease in vehicular emissions. Furthermore, AAE increased during the lockdown period due to reduced emissions from fossil-fuel combustion, while a smaller (−21%) decrease was observed for b_{sca} along with slight increases (6%) in SAE and SSA values, indicating that scattering aerosol properties were less affected by the decrease in vehicular emissions, as they are more dependent on regional sources and atmospheric processing. Nighttime BC emissions related to residential wood-burning were slightly increased during the lockdown period, with respect to previous-year means. On the contrary, aerosol and pollution changes during the lockdown period at Finokalia were low and highly sensitive to natural sources and processes.

Keywords: COVID-19; traffic; aerosol scattering; absorption; SSA; Greece

1. Introduction

The novel coronavirus SARS-COV-2 that was first evidenced in Wuhan, China, has evolved into the worst pandemic of the century so far due to widespread infection from late winter 2019 to this day [1,2]. On 11 March 2020, the World Health Organization (WHO) declared the coronavirus-related COVID-19 disease as a global pandemic [3] and,

progressively, nearly all countries around the world started adopting restriction measures or even complete nationwide lockdowns in order to combat the spread of the virus [4–6]. The restrictions in anthropogenic activities have remarkable effects on emissions of primary pollutants and subsequently improved the overall air quality throughout the world [7,8]. Therefore, although the role of air pollution and aerosols to the infection and mortality rates is not clearly defined yet [9–12], the global shutdown due to COVID-19 has allowed for a real-world analysis on the effects of reduced anthropogenic emissions in air pollution and aerosol properties.

Numerous studies around the world, as in China and East Asia [13–15], India [16–18], Southeast Asia [19,20], Europe [21–26], North America [27,28] and South America [29,30], have analyzed the effect of COVID-19 lockdowns in spring 2020 on concentrations of particulate matter (PM) and gaseous pollutants (NO_x , CO, O_3 , SO_2 , NH_3 , etc.). All these studies agree on an unprecedented reduction of air pollution worldwide due to drastic limitations in traffic and industrial activity [31–33]. Focusing on the AOD, a significant reduction (20–60%) was obtained in eastern China, while southeast Asia, eastern US and most European regions experienced a reduction reaching 40% [19,34,35]. However, in areas significantly impacted by seasonal biomass burning or dust aerosols, AODs may remain unaffected or even increase during the lockdown period [36,37]. Beyond gaseous pollutants and AOD, there are some studies analyzing the changes in BC concentrations during the lockdown period [26,38–42], which reported significant reductions (30–70%), but with large variability among regions. On the contrary, only a few works examined the changes in aerosol spectral absorption [43,44], while there is a lack of studies related to changes in spectral-scattering and single-scattering albedo (SSA).

Atmospheric aerosols scatter and absorb solar radiation in different ways depending on the particle size and shape, chemical composition and mixing type in the atmosphere, leading to surface cooling and atmospheric warming [45,46]. Changes in spectral-scattering (b_{sca}) and absorption (b_{abs}) may significantly affect the aerosol radiative impacts and alter the relative importance between surface cooling and atmospheric warming [47,48]. However, a recent study revealed only a transient and statistically insignificant direct aerosol radiative forcing of -2 to -44 mWm^{-2} over the globe during the 2020 lockdown period, which, however, can be higher over urban/industrial areas [49]. Therefore, the determination of changes in spectral-scattering and absorption during the period of COVID-19 lockdown can help understand the effect of anthropogenic activities. Specifically, in Athens, Greece, fossil-fuel combustion and residential wood-burning (RWB) emit large amounts of carbonaceous aerosols (organic carbon, OC; black carbon, BC) and gaseous pollutants [50–54], which affect the spectral-scattering and absorption properties [55,56].

In this study, we analyze the impact of the restriction measures during the COVID-19 lockdown on spectral aerosol scattering and absorption coefficients, as well as on the single-scattering albedo (SSA), using in situ measurements in urban-background Athens, Greece. Furthermore, a comparative assessment with the regional, remote site of Finokalia, Crete, is performed in order to evaluate the impact of local emissions on urban aerosol optical characteristics. The examined aerosol properties are of high importance for assessing effects on the radiation budget. The average b_{sca} , b_{abs} , SSA, SAE, AAE values during the lockdown period were compared with their pre- and post-lockdown levels as well as with the same periods in the preceding years. Moreover, meteorological observations were used to assess the relative impact of meteorology against that attributed to changes in anthropogenic emissions. To our knowledge, this is the first study that evaluates the effects that restrictions in vehicular movement, transportation and, in general, in anthropogenic activities had on aerosol scattering and absorption properties in the Mediterranean.

2. Study Area, Instrumentation and Methodology

From 23 March 2020, a total lockdown was implemented in Greece, with restrictions in the mobility of private vehicles and public transportation that lasted to 3 May. Since 4 May, when the unrestricted mobility of citizens within the regional administrative boundaries

was again allowed, to the end of May, some of the restriction measures have been progressively relaxed [40]. In the present study, we considered as lockdown period the time from 23 March to 3 May, which includes the period with the strictest restrictions in transportation and movement of private vehicles, given that one week later (11 May), the majority of commercial facilities re-opened and many citizens returned to work [40,57]. In order to assess the impact of the lockdown, the aerosol spectral-scattering and absorption properties were compared against pre- (1–22 March 2020) and post-(4–31 May 2020) lockdown periods. In addition, in order to eliminate seasonality effects, the aerosol properties in these three sub-periods of spring 2020 were compared with respective means during the previous years (2017–2019 or 2016–2019 for absorption).

Nephelometer and aethalometer measurements in Athens were performed at the Thissio Air Monitoring supersite (Figure 1), which is located atop a hill in the center of the Athens basin (37.97° N, 23.72° E, 105 m a.s.l.) and is considered representative of urban background conditions in central Athens [58]. The site is surrounded by the Acropolis and Pnyx hills and a low-density residential area in its south and west, while the nearby traffic emissions are rather limited since the city center and main avenues are at a distance of more than 500 m.



Figure 1. Overview of the study region (a). Locations of the Thissio urban background site, within the Greater Athens Area (GAA—b), and the Finokalia (FKL—c) regional background site, on the island of Crete. Taken from Google Earth.

Spectral-scattering aerosol coefficient ($b_{\text{sca}(\lambda)}$) values (between 7° and 170°; in Mm^{-1}) were measured at Thissio by means of a 3-wavelength (450, 550, 700 nm) TSI 3563 Integrating nephelometer (1 min resolution), covering the period 1 March–31 May 2020, as well as the same time frames in 2017–2019. The instrument operates at a relative humidity (RH) below 50% using a processor-controlled automatic dryer for preventing aerosol hygroscopicity effects that may increase particle scattering and modify the spectral-scattering dependence [59]. The nephelometer measurements were corrected for angular truncation errors following Anderson and Ogren [60], while the instrument was regularly calibrated using CO_2 as high span gas and air as low span gas [56]. The overall uncertainty in $b_{\text{sca}(\lambda)}$ is considered to be about 7% [61,62]. It should be noted that during all study periods, the $b_{\text{sca}(\lambda)}$ values were above 1 Mm^{-1} at all wavelengths, a threshold below which the instrumental noise becomes high [63].

Spectral absorption ($b_{\text{abs}(\lambda)}$) measurements at Thissio were performed using an AE-33 aethalometer at 7 wavelengths (370, 470, 520, 590, 660, 880 and 950 nm) and at 1 min resolution covering the spring seasons of 2016–2020. The $b_{\text{abs}(\lambda)}$ values were computed from the derived e-BC measurements using the mass absorption cross-section recommended by the manufacturer at each wavelength [64]. Furthermore, the source-specific components of BC, related to fossil fuel (BC_{ff}) and wood-burning (BC_{wb}), were computed using the biomass burning fraction (BB%), automatically provided by AE-33 that internally applies the aethalometer model [64,65].

Aethalometer (AE-33) measurements of BC and source-apportioned fractions (BC_{ff} and BC_{wb}) were also measured at the regional background station in Finokalia, Crete (Figure 1) during March–May 2020, as well as in the previous years (2016–2019), following the same procedure described above for Athens. Furthermore, during the same period, spectral b_{sca} values were monitored at Finokalia with an integrating nephelometer (Aurora-3000 Ecotech, Melbourne, Australia) at three wavelengths (450, 525 and 635 nm). Calibrations were performed regularly using CO_2 as high span gas and zero particle air as low span gas. The measurements were also corrected for angular non-idealities [66]. During periods that Aurora-3000 was not operating, a similar single wavelength (525 nm) Integrating nephelometer (Aurora-1000 Ecotech, Melbourne, Australia) was used under the same operation protocol, however, providing only total scattering measurements. A few studies in the past have examined the near-surface aerosol scattering and absorption properties at this remote coastal site [67–69].

Using the spectral b_{sca} and b_{abs} measurements, we computed intensive aerosol optical properties related to particle size and shape of aerosols (scattering Ångström exponent—SAE), to aerosol chemical composition and sources (absorption Ångström exponent—AAE) and to the relative contribution of scattering and absorption to total aerosol extinction (single scattering albedo—SSA). SAE was computed in the spectral band of the nephelometer (450–700 nm), while AAE at 470–950 nm. The spectral-scattering at the 450–700 nm band was initially fitted by a 2nd order polynomial curve in log–log coordinates, i.e., $\ln b_{\text{sca}(\lambda)} = A_2 * (\ln \lambda)^2 + A_1 * (\ln \lambda) + A_0$, since it was found to exhibit a slight curvature rather than a first-order linear wavelength dependence. The accuracy of the polynomial fitting in the 450–700 nm band was verified by the strong relationship between A_2 - A_1 and SAE (slope: 1.03; $R^2 = 0.99$; [70]). The second-order polynomial was used to extrapolate the nephelometer wavelengths to the aethalometer spectrum 370–950 nm [71]. Therefore, the spectral b_{sca} values were computed at the seven AE-33 wavelengths, and by combining the spectral-scattering and absorption values, the SSA was also estimated at 7 wavelengths. Errors in these computations can be attributed to measurement uncertainties in b_{sca} and b_{abs} , as well as to uncertainties in the extrapolated b_{sca} for wavelengths shorter than 450 and longer than 700 nm. These intensive aerosol properties were analyzed only in Athens, on an hourly basis.

In addition, hourly meteorological data (ambient temperature, RH, pressure, solar radiation, precipitation, wind speed and direction) were obtained during the examined spring periods (2016–2020) from the meteorological stations located nearby the sampling sites. Analysis of aerosol properties at both locations was performed for the same sub-periods, on an hourly basis, while in all cases, the statistical significance of the differences in aerosol properties between the examined periods was checked with t-tests at the 95% confidence level (C.L.).

3. Results and Discussion

3.1. Aerosol and Pollutant Changes at the Remote Background Site (Finokalia)

Previous works conducted in Athens have shown that a significant part of the aerosol load is due to regional sources [50–53]. In this respect, before focusing on the Athens urban environment, we examined the variability of b_{sca} and BC components at the regional background site of Finokalia, Crete (Figure 2), in March–May 2020 with respect to previous years (2016–2019). The results show a remarkable fluctuation in the b_{sca} values during the

spring periods of 2016–2019, mostly due to strong influence from Saharan dust storms, which are very frequent in this time of the year and are often characterized by extreme intensity, as it was, for example, observed in March 2018 [72]. Therefore, the large b_{sca} peaks on certain days due to natural causes could possibly mask the effects of changes in anthropogenic emissions. However, during the lockdown period, it can be seen in the graph that the b_{sca} time-series was mostly within the shaded area corresponding to the standard deviation of the 2016–2019 mean. On the contrary, the BC levels did not significantly change during the lockdown period with respect to the 2016–2019 mean, showing an increase by only 5% (0.20 to 0.21 $\mu\text{g m}^{-3}$; statistically non-significant), while the BC_{wb} levels remained low ($<0.15 \mu\text{g m}^{-3}$) throughout the examined period (Figure 2d). However, on days with intense dust storms like on 22 March 2018, BC presented peak levels, which are likely attributed to dust absorption, along with stagnant conditions of enhanced pollution since both BC_{ff} and BC_{wb} exhibited peaks [73]. This is also seen for few days in 2020, despite the low BC levels ($<0.6 \mu\text{g m}^{-3}$), as, for example, during 14–18 May 2020 when a Saharan dust episode affected Greece along with an unprecedented for that season heatwave [40], Mean BC concentrations exhibited a declining trend from pre-lockdown-to-lockdown (-11%) and from lockdown to post-lockdown (-2%). Additional analysis also showed low variability in gaseous pollutant concentrations during the lockdown period compared to pre-lockdown (-10% for NO_2 , -1% for CO and $+4\%$ for O_3). Overall, the remote site of Finokalia received negligible influence by the COVID-19 lockdown to aerosol scattering and BC absorption, which could indicate limited variability in the regional aerosol sources for the lockdown period compared to the 2016–2019 mean.

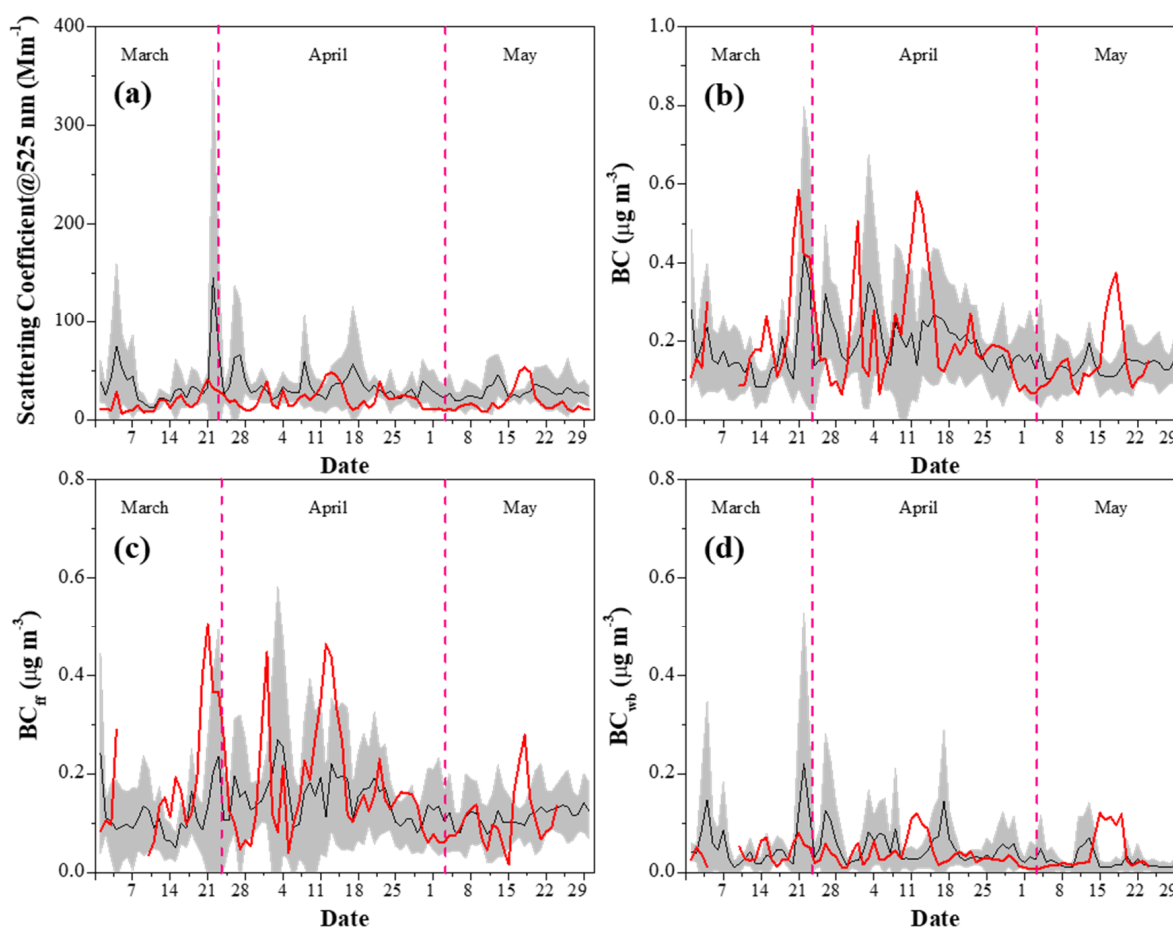


Figure 2. Daily variation of the scattering coefficient (a), black carbon (BC) (b), BC_{ff} (c) and BC_{wb} (d) concentrations at Finokalia, Crete during March–May of 2016–2019 (black) and in 2020 (red). The gray area corresponds to the standard deviation of each parameter during 2016–2019.

3.2. Meteorological Conditions in Athens during the Spring Season

Changes in meteorological parameters and boundary-layer dynamics may significantly affect the amount, types and properties of aerosols and mask the effect of changes in emissions [74,75]. Figure S1 shows the variability in the meteorological parameters at Thissio in spring 2020 (pre-, post- and lockdown periods) compared with those during the previous years.

The average air temperature during the lockdown period was slightly lower with respect to the 2016–2019 mean (-9.7% ; statistically significant at 95% confidence level). RH showed larger variability with a slightly higher mean value in 2020 (1.5%), while the solar irradiance generally followed the 2016–2019 mean (Figure S1). The average wind speed (WS) in the lockdown period was 3.0 ms^{-1} , slightly higher (7.2%; statistically significant) compared to the 2016–2019 mean (2.9 m s^{-1}). More details about the variability and relative changes in meteorological parameters between the lockdown period and previous years can be found in Grivas et al. [40].

The wind-rose patterns for b_{sca} and b_{abs} were also used to compare the wind-vector dependence of aerosol properties during the lockdown and similar periods in previous years (Figure S2). The results showed that the highest $b_{\text{sca},550}$ and $b_{\text{abs},520}$ levels during the lockdown were associated with low $WS < 3 \text{ ms}^{-1}$, similarly to previous works [56,76]. A mostly similar pattern was observed for $b_{\text{abs},520}$ in the previous years, while enhanced values from southern directions and for WS of $4\text{--}6 \text{ ms}^{-1}$ were observed for $b_{\text{sca},550}$ due to intense dust intrusions from the south, such as that on 25–27 March 2018 [77]. Therefore, the distributions of b_{sca} and b_{abs} values in the wind roses did not significantly change, apart from the lower levels due to lower emissions during the lockdown period.

3.3. Changes in Aerosol Scattering and Absorption Properties in March–May

A comparative analysis of the hourly time-series of aerosol scattering ($b_{\text{sca},550}$) and absorption ($b_{\text{abs},520}$) coefficients between March–May 2020 and the years 2016/2017–2019 in Athens is shown in Figure 3. The mean $b_{\text{sca},550}$ and $b_{\text{abs},520}$ values are given for each period, and the results show a notable decrease in $b_{\text{abs},520}$ during the lockdown period ($15.3 \pm 13.8 \text{ Mm}^{-1}$) compared to pre-lockdown ($25.2 \pm 26.9 \text{ Mm}^{-1}$), corresponding to an average reduction of -39% (statistically significant at 95% C.L.). In addition, the $b_{\text{abs},520}$ (15.3 Mm^{-1}) during the lockdown period, was notably lower (29–54%) than the respective periods in all the previous years ($22\text{--}28 \text{ Mm}^{-1}$). On the contrary, the reduction in $b_{\text{sca},550}$ during the lockdown was much lower (-15% ; statistically significant) compared to pre-lockdown and with respect to previous years (-12% to -25%). It should be noted that the decrease in $b_{\text{sca},550}$ during lockdown with respect to pre-lockdown is similar to the respective decrease (-18%) found for $\text{PM}_{2.5}$ at the same site [40]. On the other hand, significant variability is seen in $b_{\text{sca},550}$ and $b_{\text{abs},520}$ between the spring seasons, especially for the scattering coefficient for the period 1–22 March. This is likely attributed to higher RWB emissions for heating during the beginning of March [54,56] and to more unstable meteorological conditions. During May, the atmospheric conditions in Athens are more stable, with lower levels of $b_{\text{sca},550}$ and $b_{\text{abs},520}$ (Figure 3) compared with the previous months. The progressive decrease in $b_{\text{abs},520}$ from March to May during 2016–2019, is attributed to the declining trend of the BC emissions (Figure S3), as well as to better dilution processes due to progressively increasing MLH.

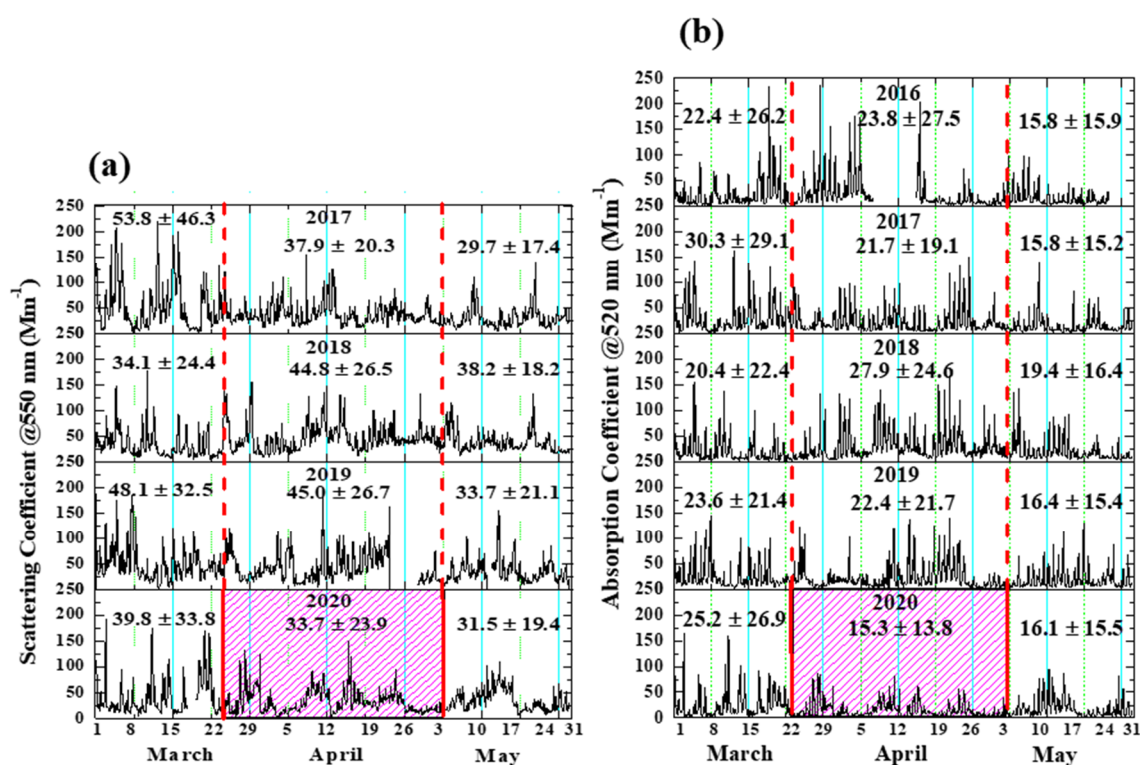


Figure 3. Time-series of hourly $b_{sca,550}$ (a) and $b_{abs,520}$ (b) during March–May for the years 2017–2020 and 2016–2020, respectively. The shaded area in 2020 corresponds to the lockdown period, and the red lines indicate periods before and after the lockdown. Mean values and standard deviations for each sub-period are mentioned in each panel.

The lower reductions in $b_{sca,550}$ than in $b_{abs,520}$ during the lockdown period can be ascribed to the wider chemical composition range of scattering aerosols (including, e.g., organics, nitrate and sulfate) in Athens. Secondary and regionally transported aerosols, which are mostly of scattering nature [78,79], comprise large fractions of $PM_{2.5}$ concentrations, reaching up to 50% during the summer period [50,52,53]. Continuous monitoring of $PM_{2.5}$ samples at Thissio and analysis of chemical composition using ion chromatography and EC/OC thermal/optical analysis [53,76] revealed that during April 2020 (lockdown period), the mean concentrations of OC and SO_4^{2-} were $3.4 \mu g m^{-3}$ and $2.7 \mu g m^{-3}$, respectively. Although OC levels were very close to the long-term (2014–2019) monthly mean of $3.3 \mu g m^{-3}$, sulfate was lower than the 2014–2019 mean of $3.7 \mu g m^{-3}$ (unpublished results). This decrease would account for $\sim 3 Mm^{-1}$ according to the parametrization of Kalivitis et al. [69], thus explaining a large part of the reduction in b_{sca} . Although the inorganic species and a large fraction of organic aerosols in urban background Athens are highly water-soluble [53,80,81], the scattering measurements were regulated for $RH < 50\%$ levels and, therefore, the water uptake cannot inflate the b_{sca} [59]. Similarly, at the regional background Finokalia site, the regional scattering aerosols did not present important changes, on average, during the lockdown period, and their presence was attributed to natural rather than anthropogenic sources. This justifies the larger reduction in absorption than in scattering in Athens, a fact also supported by a $\sim 50\%$ decrease in mean elemental carbon (EC) concentrations during April 2020 ($0.61 \mu g m^{-3}$) with respect to 2014–2019 mean of $1.2 \mu g m^{-3}$ (unpublished results). In Athens, the principal source of BC ($\sim 80\%$) in April is from fossil-fuel combustion emissions (mainly from the traffic sector) that significantly impact the aerosol absorption [54], and therefore, the drastic restrictions in the road transport sector had a large impact on lowering b_{abs} . The vast majority ($\sim 90\%$) of registered private cars in the Greater Athens Area (around 2.7 million) are gasoline-powered [82]. There are also 0.3 million trucks and buses (mostly diesel-powered) and 0.7 million 2-wheelers [83]. Based on data for traffic volumes from the Greek Ministry of Infrastructure and Transport

and Attiki Odos (the intra-city major tollway), the mean weekly vehicular traffic was reduced by about 40–70% during the lockdown period with respect to the same period in the previous two years [40,84].

A recent study has shown that the traffic-related pollutants in central Athens presented an important decrease during the lockdown period (32% for NO_2 , 35% for CO and 33% for BC_{ff}) compared with the pre-lockdown period [40]. These are comparable to the presently reported for $b_{\text{abs},520}$ (−39%). The CO emissions during the non-heating period in Athens originate from the traffic sector and mainly from private vehicles [85,86]. On the other hand, NO_2 is also a precursor of nitrate (NO_3^-) aerosols, which are considered as strongly scattering particles [55,87], and the reduction in their concentrations during the lockdown period is partly reflected in the lower $b_{\text{sca},550}$ values, along with primary organics and sulfates. Therefore, the reduction in $b_{\text{sca},550}$ during the lockdown period, should also be mainly attributed to lower primary emissions of aerosols related to the traffic sector.

The PM and gaseous pollutant concentrations were found to increase in the post-lockdown period due to the re-opening of the economy and the progressive escalation in traffic and human activities [40]. On the contrary, $b_{\text{sca},550}$ and $b_{\text{abs},520}$ presented only marginal differences (± 4 –5%) compared to lockdown, as they are significantly affected by the seasonality, regional background conditions and long-range transport of aerosols, mostly in the case of $b_{\text{sca},520}$. Therefore, in all the examined years, the $b_{\text{sca},550}$ on May 4–31 was lower than the preceding period (23 March–3 May), indicating a declining seasonal trend in scattering aerosols during the spring season in Athens. However, the mean decrease (Figure 3a) compared to the previous period was less pronounced in 2020 (2.2 Mm^{-1} against 9.4 Mm^{-1} during 2017–2019 on average). A similar feature can be observed for $b_{\text{abs},520}$ with significantly lower values by the end of spring during 2016–2019, as opposed to the slight increase in 2020 due to the notable increase in traffic emissions (Figure 3b). A photochemical pollution event and a concurrent Saharan dust transport episode during 14–18 May 2020, which increased the NO_2 production and dust levels in Athens [40], slightly affected the $b_{\text{sca},550}$ values (Figure 3a). The effect of this event was also detected at Finokalia (Figure 2), indicating its regional character. The $b_{\text{sca},550}$ and $b_{\text{abs},520}$ levels along with the intensive aerosol properties (SAE, AAE, SSA) in the examined periods, the differences between lockdown and periods before and after it, as well as with respect to previous years, are summarized in Suppl. Tables S1 and S2.

Figure 4 shows the correlations between $b_{\text{sca},550}$ and $b_{\text{abs},520}$ values for the pre-lockdown (a) and lockdown (b) periods in 2020, compared with the same periods in 2017–2019. In general, the graphs present considerable scatter ($R^2 = 0.36$ – 0.47). The correlations are significantly lower than those observed at other sites in the Mediterranean, where they are generally higher than $R^2 = 0.7$ [88–91]. The larger scatter in Athens during the spring season is likely attributed to the variety of aerosol sources, both natural and anthropogenic, and to the effect of transported dust that disproportionately increases the b_{sca} compared to the b_{abs} [62,92]. In addition, there were cases of enhanced $b_{\text{abs},520}$ for very low $b_{\text{sca},550}$ ($< 20 \text{ Mm}^{-1}$) values during 1–22 March of 2017–2019 (Figure 4a). On the contrary, the appearance of scatter plots notably changed during the lockdown period, with a much stronger correlation ($R^2 = 0.70$) between $b_{\text{sca},550}$ and $b_{\text{abs},520}$ values, which reflects a more homogeneous atmospheric composition within the Athens basin and a considerable decrease in absorption peaks. Simultaneously, at Finokalia, b_{sca} and b_{abs} were highly correlated ($R^2 = 0.80$). However, in the case of the regional background site, similar correlations ($R^2 = 0.69$ – 0.80) were also observed for the pre-lockdown period and for previous years, indicating the homogeneity of regionally transported aerosol types during the spring season.

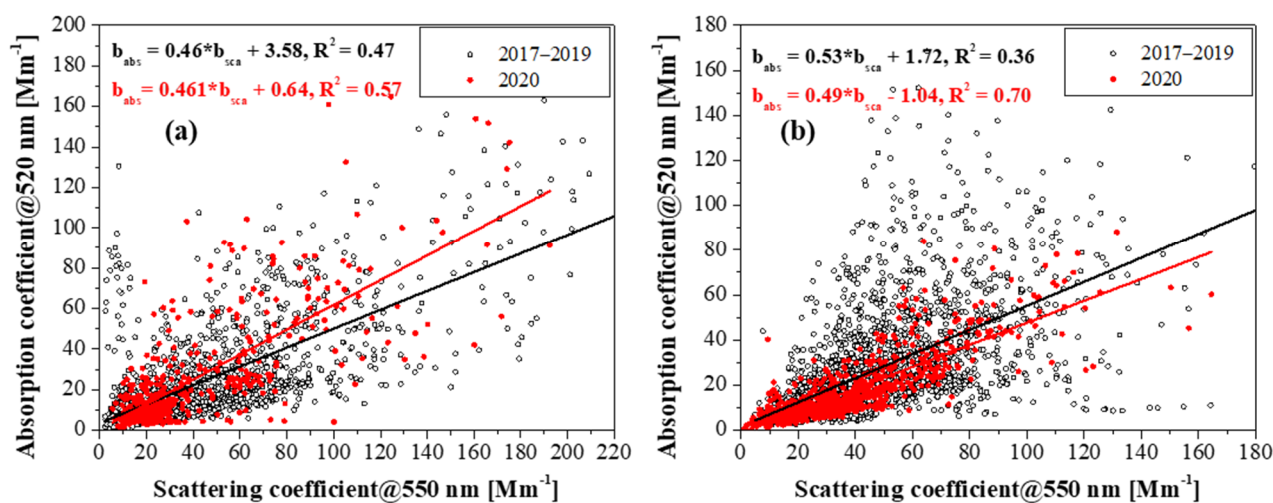


Figure 4. Correlation between scattering and absorption coefficients for the March 1–22 (a) and 23 March 23–4 May (b) periods of 2017–2019 and 2020.

3.4. Changes in Intensive Aerosol Properties

Figure 5 presents the hourly time-series of $SAE_{450-700}$, $AAE_{470-950}$ and SSA_{520} for the spring seasons of 2020 and previous years and the mean values of each sub-period. The high SAE (mostly between 1.9 and 2.0) and the low SSA (0.66 to 0.72) values in all years indicate dominance of fine-absorbing aerosols associated with fossil-fuel combustion (AAE ranges mostly between 1.2 and 1.3) in spring and almost an absence of dust near the surface [93]. Recently, Kaskaoutis et al. [70] reported that the BC-dominated aerosol type that represents the traffic conditions in central Athens dominates in spring with a fraction of around 90%.

The changes in SAE values (Figure 5a) between the different spring seasons (2017–2020) are generally larger than the slight increase observed during the lockdown period (+11.2% compared to pre-lockdown and +6.1% with respect to previous years; Tables S1 and S2). The slightly larger SAE (2.08 ± 0.26) during the lockdown is likely attributed to a smaller impact from transported dust (note the small SAE values during March 2018 due to several dust storms) and probably to less road dust resuspension due to restrictions in traffic. On the other hand, AAE presents a rather smooth, progressively declining trend from the beginning of March to the end of May (Figure 5b), which is attributed to the decreasing heating demand and the reduction in emissions from residential biomass burning [54]. In 2020, the large decrease in traffic-related absorbing particles, as a consequence of the drastic restrictions, led to higher AAE values (6.3%; statistically significant) during the lockdown period compared to the 2016–2019 mean (Table S1), taking in mind the low AAE values (1.0–1.1) of particles from vehicle exhaust emissions [94–96]. Furthermore, a slight intensification of wood-burning emissions was observed on certain nights during the lockdown period that may have also contributed to the increase in AAE, as will be analyzed in the next section. Finally, SSA_{520} appeared relatively stable during the spring seasons (Figure 5c). During the lockdown period, SSA_{520} slightly increased by 5.9% with respect to the 2017–2019 means and by 9.1% compared to pre-lockdown (Tables S1 and S2). However, in the latter case, the decrease in wood combustion between the pre-lockdown and lockdown periods may affect the results. Overall, the increase in SSA during the lockdown period reflects the larger reduction in levels of highly absorbing BC aerosols from vehicular emissions rather than of scattering-type aerosols [97,98].

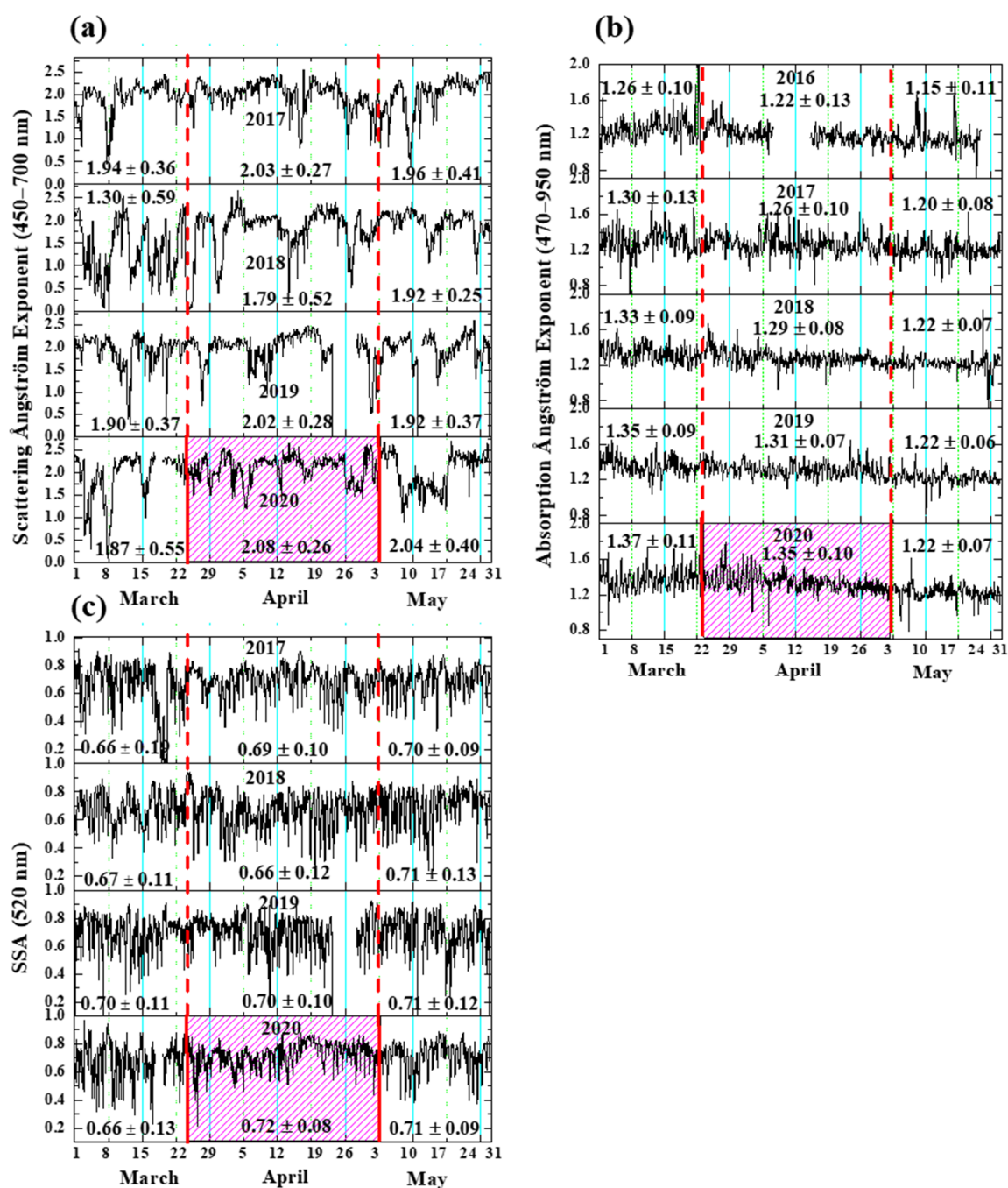


Figure 5. Time-series of hourly scattering absorption exponents (SAE) (a), Ångström absorption exponents (AAE) (b) and single-scattering albedo (SSA) (c) values during March–May for the years 2017–2020 (2016–2020 for AAE). The shaded area in 2020 corresponds to the lockdown period, and the red lines indicate periods before and after the lockdown. Mean values and standard deviations for each sub-period are mentioned in each panel.

3.5. Changes in Diurnal Aerosol Patterns during Lockdown, Pre- and Post-Lockdown Periods

In order to evaluate the changes in extensive and intensive aerosol properties and their dependence on the lockdown restrictions, the mean diurnal patterns in the examined periods of 2020 are compared against those of the 3–4 previous years. Figure 6 shows the mean diurnal cycles of $b_{\text{sca},550}$ and $b_{\text{abs},520}$ in 2020 for pre-, post- and lockdown periods compared with the respective means in 2016/2017–2019, while similar graphs were produced for $\text{SAE}_{450-700}$, $\text{AAE}_{470-950}$ and SSA_{520} (Figure 7), as well as for the BC components (Figure S3).

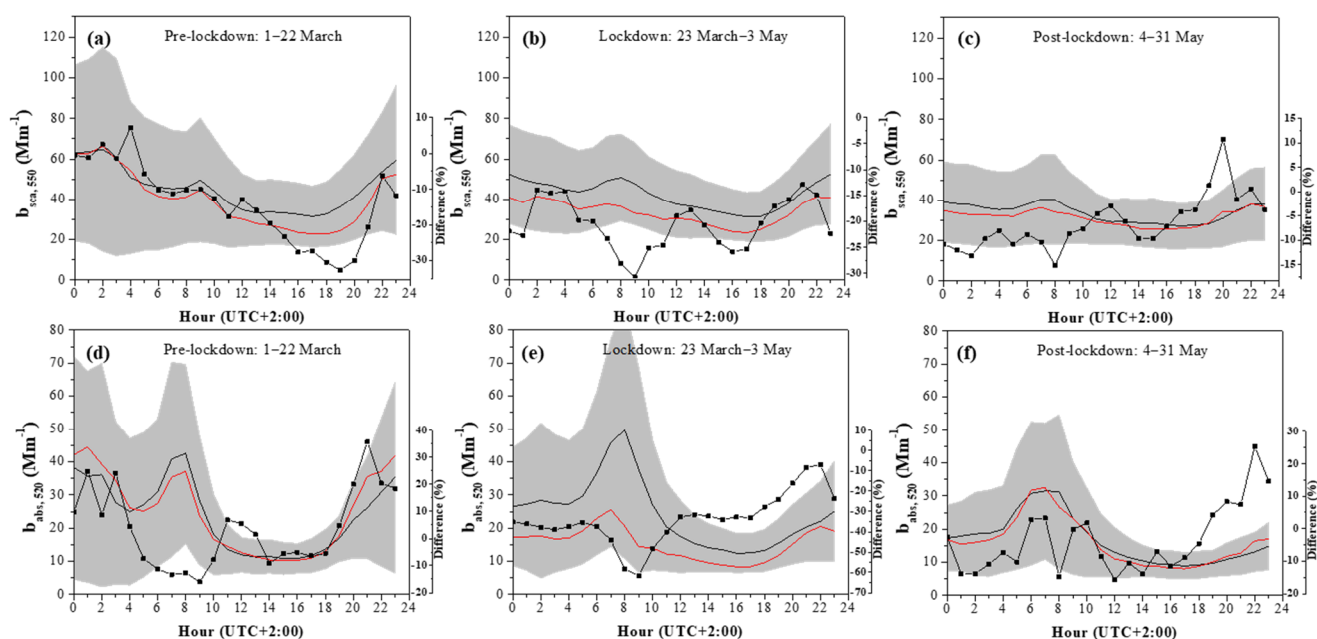


Figure 6. Mean diurnal variation of $b_{sca,550}$ (a–c) and $b_{abs,520}$ (d–f) for periods pre-, post- and during the lockdown. Red line corresponds to 2020, while the black line represents the mean for the years 2017–2019 for scattering and 2016–2019 for absorption. The shaded area corresponds to one standard deviation from the hourly mean during 2016–2019 and/or 2017–2019. The percentage (%) differences in $b_{sca,550}$ and $b_{abs,520}$ between the examined periods in 2020 and the mean of previous years are also shown.

The most regional character of scattering aerosols in Athens is supported by the rather weak diurnal patterns of $b_{sca,550}$ for all periods, since morning traffic peaks are nearly absent, while the changes between pre- and post-lockdown periods were small (mostly within $\pm 10\%$) (Figure 6a,c). Lower vehicular emissions and road dust resuspension in morning hours (08:00–09:00 LST) [56] did not influence $b_{sca,550}$ much (Figure 6b), indicating a weak impact of direct traffic emissions on aerosol scattering.

Although $b_{abs,520}$ diurnal cycles in 2020 closely follow the 2016–2019 means in pre- and post-lockdown periods (Figure 6d,f), the traffic restrictions during lockdown lead to significant differences throughout the day, reaching -60% in the morning traffic hours (Figure 6e). In all examined periods, the morning traffic peak in absorption clearly prevails, while during the lockdown, the traffic peak appears largely reduced and an hour earlier (07:00 LST) (Figure 6e), probably due to the absence of go-to-work traffic congestion. Similarly, a flat diurnal cycle of BC was noticed in Suzhou, Yangtze River Delta, China during the lockdown period, indicating the remarkable decrease in traffic and the disappearance of the morning and evening traffic-related peaks [41]. During the lockdown night hours, $b_{abs,520}$ displayed much lower decrease fractions (about 10% with respect to previous years), as the decrease in nighttime traffic emissions is somewhat counterbalanced by a slight intensification of wood combustion. This is also supported by the observed BC_{ff} and BC_{wb} diurnal patterns (Figure S3). During the post-lockdown period, $b_{sca,550}$ levels were mostly similar to slightly lower than during lockdown, while $b_{abs,520}$ was again increased in the morning hours, signifying the free circulation of vehicles. The decrease in the $b_{sca,550}$ and $b_{abs,520}$ at noon and early afternoon hours, is attributed to boundary-layer dynamics related to a deeper MLH [99].

The average diurnal cycles of $SAE_{450-700}$ do not exhibit pronounced variability during the examined periods. In 2020, higher SAE values can be seen throughout the day (but not more than 15%) with respect to the 2017–2019 means (Figure 7a–c). Apart from a marginal SAE decrease during daytime in pre-lockdown, these mostly constant diurnal patterns imply small changes in aerosol size distribution or in the fine-to-coarse mode

ratio, indicating a predominance of fine anthropogenic aerosols throughout the spring season [56,100,101]. Furthermore, the SAE changes during the lockdown period remain nearly constant (4–12%) throughout the day, indicating a limited effect from changes in the traffic sector.

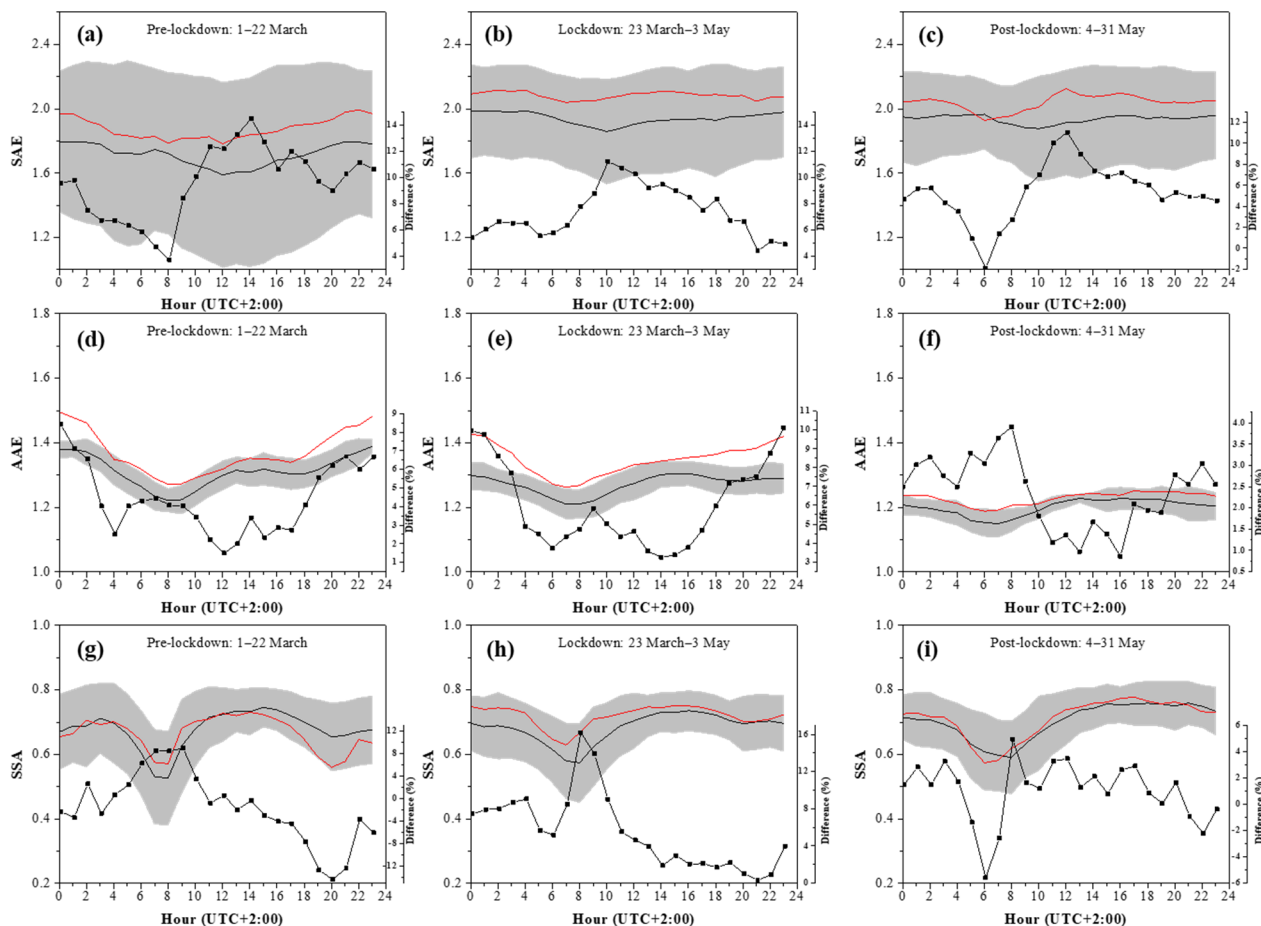


Figure 7. Mean diurnal variation of $SAE_{450-700}$ (a–c), $AAE_{470-950}$ (d–f) and SSA_{520} (g–i) for periods pre-, post- and during the lockdown. Red line corresponds to 2020, while the black line represents the mean for the years 2017–2019 for SAE and SSA and 2016–2019 for AAE. The shaded area corresponds to one standard deviation from the hourly mean during 2016–2019 and/or 2017–2019. The percentage (%) differences in SAE (scattering Angström exponent), AAE (absorption Angström exponent) and SSA (single scattering albedo) between the examined periods in 2020 and the mean of previous years are also shown.

AAE values closely follow the 2016–2019 diurnal pattern, but they exhibit higher (within 10%) values during 2020 (Figure 7d–f). Despite this small relative increase, the AAE values during the lockdown period were at the upper limits of- or beyond- the shaded area that defines 1 standard deviation of the 2016–2019 mean. It is also characteristic that the highest (%) increase in AAE during the lockdown period is observed during the night hours due to the combined effects of the decrease in evening traffic and the increased RWB emissions from fireplaces on certain days of the lockdown period. On the other hand, secondary organic aerosol (SOA) may slightly contribute to the increase of AAE around midday in all examined periods, following the minimum AEs observed during the traffic rush hours (around 09:00 LST) (Figure 7d–f). The OC/EC ratio is commonly used to empirically discern between primary and secondary OC, estimating the primary and secondary organic carbon fractions (POC and SOC, respectively), using the EC tracer method in Athens [50,70,102]. The mean OC/EC ratio in $PM_{2.5}$ was 6.2 in April 2020, compared to 2.9, averaged for April during 2014–2019 [53,103]. The large increase of the

OC/EC ratio can be attributed to the smaller impact of primary combustion emissions and an enhanced presence of secondary organic aerosol [99,104]. Similarly, the increased organic aerosol fraction has been associated with larger values of AAE and SAE in Rome [105]. Chatterjee et al. [106] reported higher SOA formation during the lockdown in the eastern Indian Himalayas due to reduced NO and high concentrations of O₃ and biogenic VOCs, implying that the site characteristics and the relative fraction between urban/anthropogenic and biogenic VOCs are especially important for the SOA formation processes during the lockdown period.

The steep decrease in SSA values during the morning rush traffic hours in all the examined periods (Figure 7g–i) reflects the strong impact of highly absorbing BC aerosols from vehicular combustion [90,107,108]. Following the morning minima, SSA displays an increasing tendency and a large plateau of higher values around noon to afternoon, which is likely ascribed to SOA formation that may increase SSA, as these particles are more efficient scatterers [56,98]. This large plateau continues to the evening/night hours in the post-lockdown period, while conversely, the enhanced RWB emissions at the beginning of March (pre-lockdown period) result in a decrease of SSA during the late evening hours due to absorbing OC from wood combustion [70,108,109]. Previous research in Athens has shown that SSA decreased with increasing BC/PM₁ ratio, while it remained practically unaffected by changes in the organic component [70]. This can explain the decrease in SSA during the morning traffic hours in all periods and the mostly neutral diurnal cycle in the rest of the day. During the lockdown period, SSA was always larger than the 2017–2019 mean, with the highest difference detected in the morning traffic hours (14–16%) due to the higher relative decrease in absorption than scattering (Figure 7h).

Supplemental Figure S3 presents the diurnal variations of the BC, BC_{ff} and BC_{wb} concentrations for the examined periods in 2020 against the mean diurnal patterns of the preceding years. The BC_{ff} component showed a considerable decrease during the lockdown period (−25% to −40%), which maximized (−65%) during the morning traffic hours (08:00–9:00 LST) with respect to the 2016–2019 mean. On the contrary, the BC_{wb} presented a continuous decreasing trend from March to May, while its levels in 2020 were above the 2016–2019 mean in the evening and night hours during the pre-lockdown period, while in lockdown and post-lockdown, BC_{wb} levels were mostly within the range of the 2016–2019 means. The enhanced BC_{wb} concentrations on certain days during the lockdown period (mainly at night hours) are attributed to escalated emissions from the residential sector due to higher demand for heating (also using fireplaces) from people staying or even working indoors [25].

3.6. Modifications in Spectral Aerosol Scattering and Absorption

This section examines the changes in spectral aerosol scattering, absorption coefficients and SSA in order to assess the lockdown effect through comparisons with the same period in previous years. The spectral aerosol properties are initially examined during the morning (06:00–10:00 LST) and evening/night (20:00–02:00 LST) hours (Figure 8), in order to quantify the effects of different emission sources, i.e., vehicular emissions during morning rush hours, traffic and biomass burning during the night [80].

The results show a very similar mean spectral dependence of scattering for morning and night hours during 2017–2019, with SAE means of 1.95 and 1.99, respectively. During the lockdown, the spectral b_{sca} values were reduced, more during the morning hours, but at the same rate across the spectrum, as the Ångström power-law fit ($b_{\text{sca},\lambda} = \beta\lambda^{-\text{SAE}}$) estimated SAE values of 2.14 and 2.16 (Figure 8a). The slightly larger SAE during the lockdown implies a higher relative decrease in spectral b_{sca} at longer wavelengths, which is likely attributed to less coarse material such as road dust due to restrictions in traffic [70]. More pronounced changes were observed in the spectral b_{abs} between morning and night hours for the lockdown and 2016–2019 periods (Figure 8b). Spectral b_{abs} maximizes during the morning hours, with a fitted AAE of 1.18 for the 2016–2019 mean corresponding to fossil-fuel combustion sources, while the mean spectral b_{abs} during night exhibits a higher

AAE = 1.33 due to enhanced emissions from RWB [99]. The modifications in the spectral b_{abs} during the lockdown period are mostly emphasized by the higher decrease during the morning hours, but with a slightly higher spectral dependence (AAE = 1.25). For the night hours during the lockdown, the spectral b_{abs} appears enhanced at shorter wavelengths ($b_{\text{abs},370}$ higher than the morning respective value), possibly indicating a stronger effect by BrC absorption (AAE = 1.52) from RWB emissions [110–112].

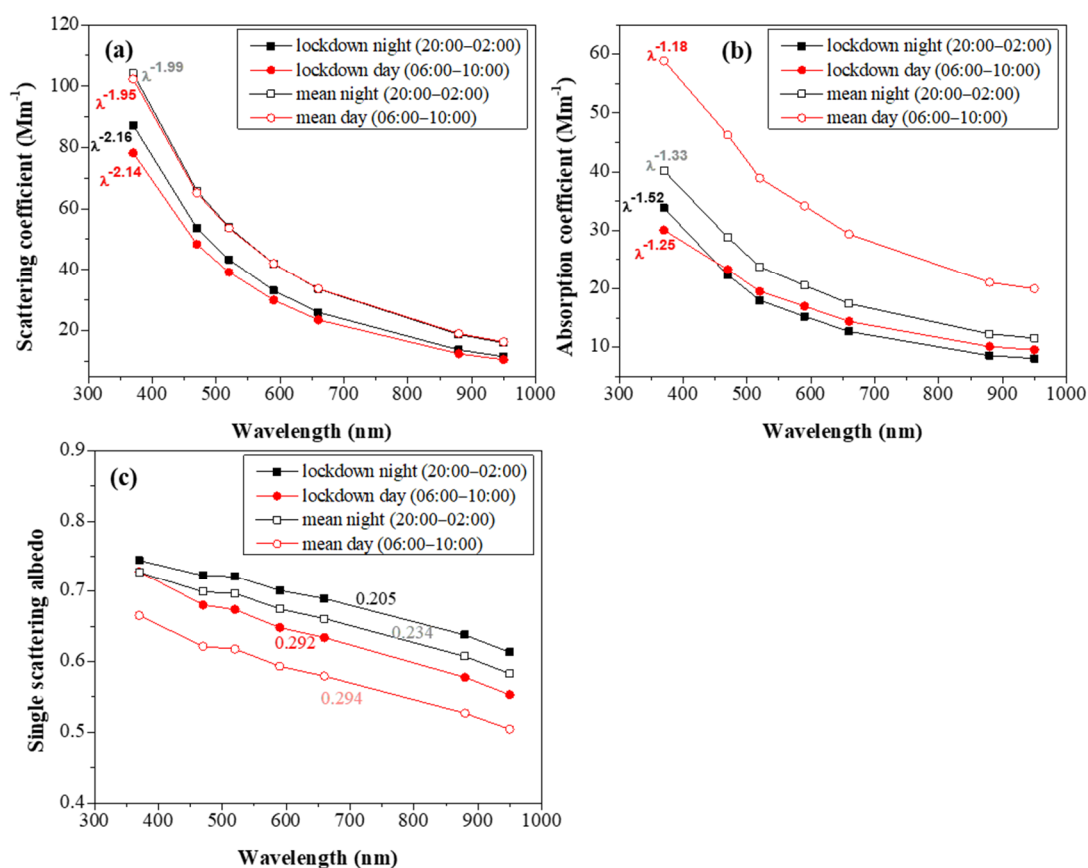


Figure 8. Spectral-scattering (a), absorption (b) and SSA (c) at night and day hours during 20 March–3 May, in 2017–2019 (2016–2019 for absorption) and in the same period in 2020 (lockdown). The averaged coefficients for the spectral-scattering, absorption as well as the Ångström exponents for the SSA are given in each panel.

SSA is an important climatic factor, and its spectral dependence has also been widely used as an indicator of aerosol types [94,113–115]. Decrease of SSA by wavelength is characteristic of urban-industrial aerosols with high BC content from fossil-fuel combustion [107,116], as these aerosols exhibit stronger wavelength dependence of scattering than absorption. On the contrary, external or internal mixing with other mostly scattering urban aerosols (organics, sulfate, nitrate) lowers the decreasing spectral SSA rate, while a high presence of BrC from biomass burning may result in $d\text{SSA}/d\lambda$ ratios close to 0, or even positive [109,117,118]. The current analysis shows a rather subtle modification in the spectral SSA for day and night hours during the lockdown period, compared to the same periods in preceding years (Figure 8c). The spectral SSA is lower during lockdown morning compared to nighttime due to the strong effect that the traffic sector still has in spite of the restrictions (Figure S3). It also exhibits a higher SSA Ångström exponent (SSAAE = 0.292) compared to night (SSAAE = 0.205). The comparison with respect to previous years reveals that the SSA during lockdown daytime is higher by ~9% than the mean due to reasons discussed above (Figures 5c and 7h), but it exhibits a similar wavelength dependence, indicating negligible changes in aerosol-type composition. The SSAAE values during night-time are slightly lower due to the higher presence of BrC, while the enhanced RWB during the

lockdown nights (mean BB% = 36%) could explain the lower SSAAE of 0.205 [118–120] since light-absorbing BrC displays lower decreasing rates of SSA at longer wavelengths compared to BC [73,121,122]. In supporting this statement, Katsanos et al. [56] found lower SSAAE values during winter compared to the other seasons in Athens due to enhanced levels of biomass-burning aerosols and a pronounced increase in SSAAE values during the morning traffic hours. Furthermore, during the same time frame (20:00–02:00 LST) of 23 March–3 May in 2016–2019, the BC_{wb} fraction was 22%, much lower than the respective one during the lockdown nights, resulting in a higher mean SSAAE of 0.234 (Figure 8c). Therefore, it is concluded that the SSAAE is rather sensitive to the relative changes between fossil fuel and wood-burning emissions [118,123].

Correlations of measured aerosol load, either as columnar AOD or as scattering and absorption coefficients, and its spectral dependence has been widely used for the identification of key aerosol types [89,91,124–126]. Therefore, an investigation of the correlations $b_{sca,550}$ vs. $SAE_{450-700}$ and $b_{abs,520}$ vs. $AAE_{470-950}$ during the lockdown and the same period in previous years can reveal modifications in atmospheric composition, attributable to changes in emission sources and not so much to seasonality. This analysis (Figure 9) shows considerable changes in the distribution of data points between scattering and absorption and between lockdown data (solid red circles) and data from previous years (open gray circles). Focusing on scattering (Figure 9a), the highest $b_{sca,550}$ values ($>80 \text{ Mm}^{-1}$) are associated with very high SAE (>2) during the lockdown period, indicating the prevalence of fine-mode aerosols in the Athens atmosphere, while there is also a higher possibility of lower $b_{sca,550}$ and higher SAE values compared to the same periods (23 March–3 May) in 2017–2019. In the previous years, several cases indicate an enhanced presence of coarse-mode dust aerosols corresponding to very low SAE values (<0.5), mostly detected during the dust events in March 2018 [77]. Cases with SAE values in the range of 0.5–1.2, which mostly imply mixing of urban background with transported coarse particles, are also absent during the lockdown period but are fairly common during the spring season [70].

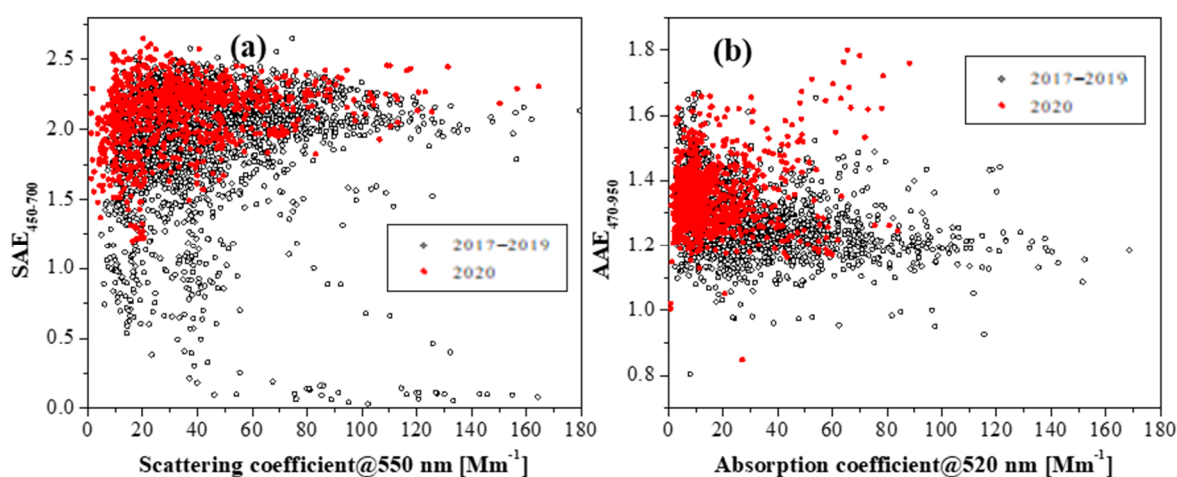


Figure 9. Correlation between b_{sca} and SAE (a) and between b_{abs} and AAE (b) during the period 23 March–3 May for the years 2017–2019 and for 2020 (lockdown).

Regarding absorption (Figure 9b), a remarkable modification of the 2017–2019 scatter plot is observed during the lockdown period, with main characteristics the accumulation of data points at lower $b_{abs,520}$ values and an enhanced AAE (>1.6) for the highest $b_{abs,520}$ values ($>50 \text{ Mm}^{-1}$). The latter indicates cases with enhanced recreational RWB emissions (e.g., fireplaces), as citizens stayed more at their houses. Another major difference between the two examined periods is the near absence of data points characterized by high $b_{abs,520}$ ($>60 \text{ Mm}^{-1}$) and AAE around 1.1–1.2 during the lockdown. These data points typically correspond to enhanced emissions from fossil-fuel combustion along with weak influence from the secondary aerosol formation. In ambient conditions, the AAE related to fossil-

fuel (normally close to 1) may be modified depending on aerosol size, BC coating and atmospheric processing [127,128] and increase up to 1.5 depending on the shell material and the lensing effect [129]. The modification of the $b_{\text{abs},520}$ vs. $\text{AAE}_{470-950}$ scatter plot indicates significant changes in the atmospheric chemical composition during the lockdown period in Athens.

The correlation between SAE and AAE values has been extensively used for the identification of key aerosol types [63,130–134] and may reveal changes in atmospheric composition during the lockdown period, able to modulate the aerosol radiative effect [135]. In this respect, Figure 10a–c shows the correlations between $\text{SAE}_{450-700}$ and $\text{AAE}_{470-950}$ for the lockdown period and for the same periods in previous years (2017–2019), aiming to explore possible changes that signify a modification in the dominant aerosol types in Athens. The variety of aerosol types in Athens leads to a high scatter in both data cases. Focusing on the SAE vs. AAE scatter plots (Figure 10a–c, the results point to a higher homogeneity during the lockdown period with an absence of data points lying in the $\text{SAE} < 1$ area (mostly super-micron aerosols). In addition, there is a higher frequency of $\text{SAE} > 1.5$ and $\text{AAE} > 1.5$, thus increasing the fraction of the mixing of brown carbon (BrC) and BC aerosol [70,131] that corresponds to wood-burning (Figure 10a). These data points are also associated with the highest $b_{\text{sca},550}$ values (Figure 10b), indicating turbid atmospheric conditions under RWB emissions on certain nights during the lockdown period (Figure S4). During 2017–2019 (Figure 10c), high $b_{\text{sca},520}$ values were mostly related to low AAE (close to 1.1) and/or to low SAE (close to zero; dust events).

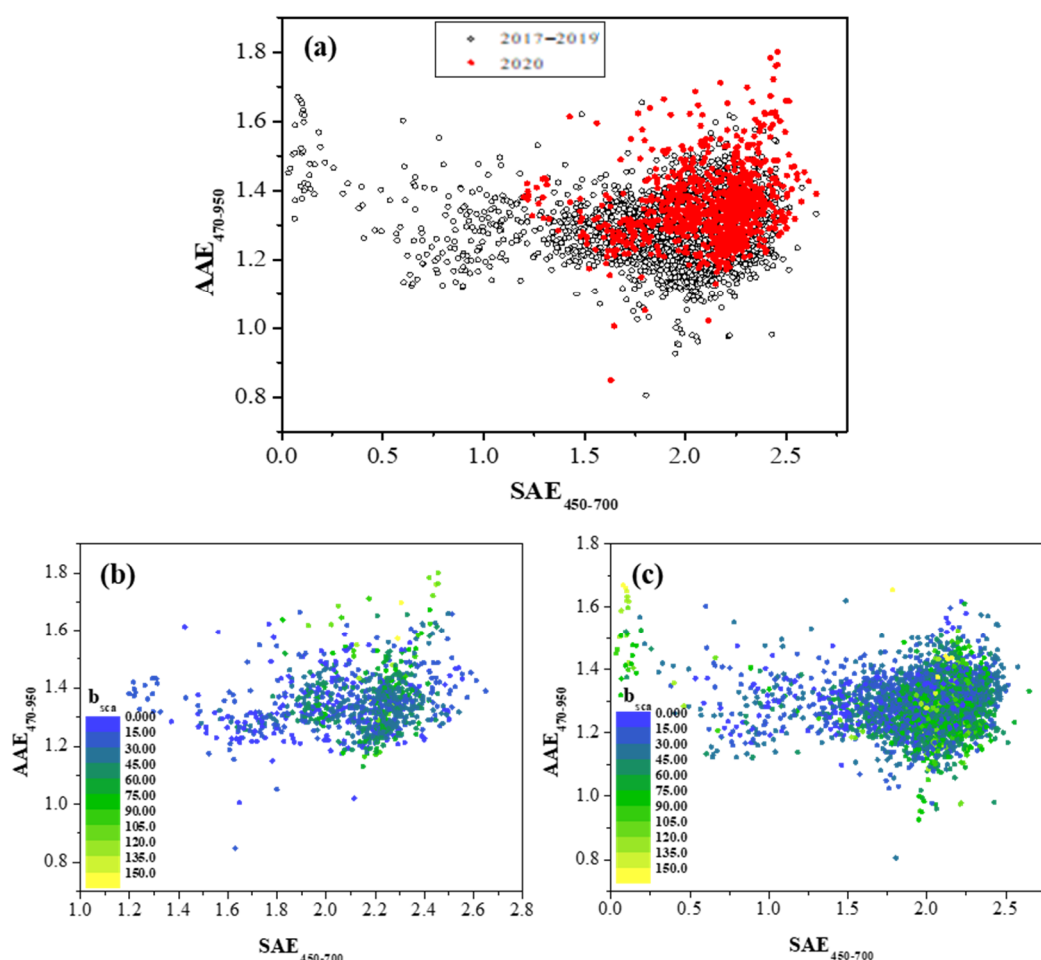


Figure 10. Correlation between SAE and AAE values during the period 23 March–3 May for the years 2017–2019 and for 2020 (a), and as a function of the $b_{\text{sca},550}$ (color scale) for the same periods in 2020 (b) and for 2017–2019 (c).

4. Conclusions

In this study, we examined the effects of the spring 2020 lockdown (23 March–3 May) on spectral aerosol scattering and absorption properties in Athens, Greece, with respect to the pre- (1–22 March) and post- (4–31 May) lockdown periods. The comparison was repeated for the same periods of the previous 3–4 years, allowing for an assessment of the effects of restriction measures on aerosol properties. Moreover, similar analyses were performed at the remote background site of Finokalia, Crete, to assess the lockdown impacts on a regional level. The analysis revealed a pronounced influence of reduced anthropogenic emissions in urban areas on aerosol properties, which in turn are closely related to radiative forcing. Remarkable changes were also observed for intensive properties related to aerosol size, shape and chemical composition, like scattering and absorption Ångström exponents (SAE, AAE) and single-scattering albedo (SSA).

At the remote site of Finokalia, the effect of lockdown did not significantly affect the b_{sca} and BC components, while the variations in scattering and absorbing aerosols were mostly attributed to natural causes like dust events. This feature was different from that observed in Athens, where the locally emitted aerosols from the traffic sector mainly affected the light absorption rather than the scattering, with morning peaks in b_{abs} being much more pronounced than those of b_{sca} . Therefore, the drastic limitation of circulation during the lockdown period caused a much larger reduction in b_{abs} (reaching ~60% during the morning hours with respect to previous years) compared with b_{sca} , which presented only a 25–30% decrease during the same time frame. Overall, the much lower mean reduction rate in scattering (−21%) compared to absorption (−36%) can be attributed to the more regional character of scattering aerosols around the greater Athens area. The absorbing properties seem to be highly related to vehicular emissions and mostly to BC from fossil fuel combustion, which also revealed a pronounced decrease reaching −65% during the morning traffic hours. On the contrary, the wood-burning BC fraction (BC_{wb}) did not present notable changes, while it was found to slightly increase during the night hours, with respect to 2016–2019 mean, as a consequence of increased emissions from residential wood-burning in fireplaces due to stay-at-home measures. In addition, the traffic restrictions affected the intensive aerosol properties in Athens, but to a lower degree, since an increase was observed for SAE (6.1%), AAE (6.3%) and SSA (5.9%) during the lockdown period with respect to previous years. This could be associated with the larger reductions in absorbing rather than scattering aerosols and lowering concentrations of resuspended road dust due to the limitation in road traffic. Consequently, the aerosol during the lockdown period in Athens was dominated by finer, less-absorbing particles and enhanced residential wood-burning emissions during nighttime.

Overall, the lower urban aerosol loading may also affect the aerosol radiative forcing (ARF), leading to smaller ARF values in the surface and top of the atmosphere due to the presence of less-absorbing aerosols during the lockdown period. These potential effects that have been considered of a transient character should be reevaluated given the renewed restriction in the second half of 2020 and in 2021. Since the start of November 2020, Greece has entered a second national lockdown, which is foreseen to extend well into the new year. Therefore, it will be challenging to extend the results of the present study, exploring possible modifications in atmospheric composition and aerosol properties and types during winter, when local pollution events are normally more frequent and more intense.

Supplementary Materials: The following are available online at <https://www.mdpi.com/2073-4433/12/2/231/s1>, Figure S1: (a) Mean daily variation of meteorological parameters in March–May of 2016–2019 (blue) and in the respective period in 2020 (orange) at Thissio, Athens. The shaded area defines the lockdown period in 2020 (23 March–3 May). (b) Mean diurnal variation of meteorological parameters in 2016–2019 (blue) and in 2020 (orange) during the March–May period, Table S1: Mean \pm standard deviation values of scattering, absorption, SAE, AAE and SSA during the pre-lockdown (1–22 March 2020), lockdown (23 March–3 May 2020) and post-lockdown (4–31 May 2020) periods and associated changes at Thissio, Athens. The asterisk denotes statistically signifi-

cant difference (0.95 confidence level), Table S2: Mean \pm standard deviation values of scattering, absorption, SAE, AAE and SSA for 2020 and previous years, corresponding to the pre-lockdown (1–22 March), lockdown (23 March–3 May) and post-lockdown (4–31 May) periods. Displaying also the % differences in 2020 compared with the mean of previous years. The asterisk denotes statistically significant difference (0.95 confidence level), Figure S2: Wind roses of the $b_{sca,550}$ (a, b) and $b_{abs,520}$ (c, d) during the period 23 March–3 May for 2016–2019 (a, c) and 2020 lockdown (b, d), Figure S3: Mean diurnal patterns of BC (a–c), BC_{ff} (d–f) and BC_{wb} for periods pre- post- and during the lockdown. Red line corresponds to the year 2020, while the black line to the period means for the years 2016–2019. The shaded area corresponds to one standard deviation from the 2016–2019 diurnal mean. The percentage (%) differences between 2020 and 2016–2019 (red and black lines, respectively) are also given.

Author Contributions: Conceptualization, D.G.K., G.G., E.L. and N.M.; methodology, D.G.K. and N.M.; formal analysis, D.G.K., N.K., G.K., P.Z., I.S. and P.K.; investigation, D.G.K., G.G., E.L. and U.C.D.; data curation, D.G.K., N.K., G.K., I.S., P.Z., U.C.D. and P.K.; writing—original draft preparation, D.G.K.; writing—review and editing, D.G.K., G.G., E.L., N.K. and N.M.; supervision, N.M. and E.G.; project administration, N.M. and E.G.; funding acquisition, N.M. and E.G. All authors have read and agreed to the published version of the manuscript.

Funding: This research was funded by the project “PANhellenic infrastructure for Atmospheric Composition and climatE change” (MIS 5021516), which is implemented under the Action “Reinforcement of the Research and Innovation Infrastructure”, funded by the Operational Program “Competitiveness, Entrepreneurship and Innovation” (NSRF 2014–2020) and co-financed by Greece and the European Union (European Regional Development Fund).

Institutional Review Board Statement: Not applicable.

Informed Consent Statement: Not applicable.

Data Availability Statement: Data are available after request.

Acknowledgments: The study received support by ERA-PLANET (www.era-planet.eu) transnational project SMURBS (www.smurbs.eu) (grant agreement no. 689443), funded under the EU Horizon 2020 Framework Program. K. Dimitriou is highly acknowledged for nephelometer data curation at the Thissio monitoring site.

Conflicts of Interest: The authors declare no conflict of interest.

References

- Lu, R.; Zhao, X.; Li, J.; Niu, P.; Yang, B.; Wu, H.; Wang, W.; Song, H.; Huang, B.; Zhu, N.; et al. Genomic characterisation and epidemiology of 2019 novel coronavirus: Implications for virus origins and receptor binding. *Lancet* **2020**, *395*, 565–574. [[CrossRef](#)]
- Shi, H.; Han, X.; Jiang, N.; Cao, Y.; Alwalid, O.; Gu, J.; Fan, Y.; Zheng, C. Radiological findings from 81 patients with COVID-19 pneumonia in Wuhan, China: A descriptive study. *Lancet Infect. Dis.* **2020**, *20*, 425–434. [[CrossRef](#)]
- World Health Organization. *Coronavirus Disease (COVID-2019) Situation Reports*; World Health Organization: Geneva, Switzerland, 2020. Available online: <https://www.who.int/emergencies/diseases/novel-coronavirus-2019/situation-reports/>. (accessed on 23 March 2020).
- Broomandi, P.; Karaca, F.; Nikfal, A.; Jahanbakhshi, A.; Tamjidi, M.; Kim, J.R. Impact of COVID-19 Event on the Air Quality in Iran. *Aerosol Air Qual. Res.* **2020**, *20*, 1793–1804. [[CrossRef](#)]
- Donzelli, G.; Cioni, L.; Cancellieri, M.; Llopis Morales, A.; Morales Suárez-Varela, M.M. The Effect of the Covid-19 Lockdown on Air Quality in Three Italian Medium-Sized Cities. *Atmosphere* **2020**, *11*, 1118. [[CrossRef](#)]
- Muhammad, S.; Long, X.; Salman, M. COVID-19 pandemic and environmental pollution: A blessing in disguise? *Sci. Total Environ.* **2020**, *728*, 138820. [[CrossRef](#)] [[PubMed](#)]
- Lal, P.; Kumar, A.; Kumar, S.; Kumari, S.; Saikia, P.; Dayanandan, A.; Adhikari, D.; Khan, M. The dark cloud with a silver lining: Assessing the impact of the SARS COVID-19 pandemic on the global environment. *Sci. Total Environ.* **2020**, *732*, 139297. [[CrossRef](#)]
- Karkour, S.; Itsubo, N. Influence of the Covid-19 Crisis on Global PM2.5 Concentration and Related Health Impacts. *Sustainability* **2020**, *12*, 5297. [[CrossRef](#)]
- Contini, D.; Costabile, F. Does air pollution influence COVID-19 outbreaks? *Atmosphere* **2020**, *11*, 377. [[CrossRef](#)]
- Conticini, E.; Frediani, B.; Caro, D. Can atmospheric pollution be considered a cofactor in extremely high level of SARS-CoV-2 lethality in northern Italy? *Environ. Pollut.* **2020**, *261*, 114465. [[CrossRef](#)]
- Srivastava, A. COVID-19 and Air Pollution and Meteorology-an intricate relationship: A review. *Chemosphere* **2021**, *263*, 128297. [[CrossRef](#)]

12. Yao, M.; Zhang, L.; Ma, J.; Zhou, L. On airborne transmission and control of SARS-Cov-2. *Sci. Total Environ.* **2020**, *731*, 139178. [[CrossRef](#)] [[PubMed](#)]
13. Wang, Q.; Su, M. A preliminary assessment of the impact of COVID-19 on environment—A case study of China. *Sci. Total Environ.* **2020**, *728*, 138915. [[CrossRef](#)]
14. Vuong, Q.T.; Thang, P.Q.; Park, M.-K.; Choi, S.-D. Effects of the COVID-19 lockdown on criteria air pollutants in the city of Daegu, the epicenter of South Korea's outbreak. *Environ. Sci. Pollut. Res.* **2020**, *28*, 1–9. [[CrossRef](#)] [[PubMed](#)]
15. Zhang, R.; Zhang, Y.; Lin, H.; Feng, X.; Fu, T.-M.; Wang, Y. NO_x emission reduction and recovery during COVID-19 in east China. *Atmosphere* **2020**, *11*, 433. [[CrossRef](#)]
16. Chauhan, A.; Singh, R.P. Decline in PM_{2.5} concentrations over major cities around the world associated with COVID-19. *Environ. Res.* **2020**, *187*, 109634. [[CrossRef](#)]
17. Kumar, S. Effect of meteorological parameters on spread of COVID-19 in India and air quality during lockdown. *Sci. Total Environ.* **2020**, *745*, 141021. [[CrossRef](#)] [[PubMed](#)]
18. Vadrevu, K.; Eaturu, A.; Biswas, S.; Lasko, K.; Sahu, S.; Garg, J.K.; Justice, C. Spatial and temporal variations of air pollution over 41 cities of India during the COVID-19 lockdown period. *Sci. Rep.* **2020**, *10*, 16574. [[CrossRef](#)]
19. Kanniah, K.D.; Kamarul Zaman, N.A.F.; Kaskaoutis, D.G.; Latif, M.T. COVID-19's impact on the atmospheric environment in the Southeast Asia region. *Sci. Total Environ.* **2020**, *736*, 139658. [[CrossRef](#)]
20. Stratoulis, D.; Nuthammachot, N. Air quality development during the COVID-19 pandemic over a medium-sized urban area in Thailand. *Sci. Total Environ.* **2020**, *746*, 141320. [[CrossRef](#)]
21. Baldasano, J.M. COVID-19 lockdown effects on air quality by NO₂ in the cities of Barcelona and Madrid Spain. *Sci. Total Environ.* **2020**, *741*, 140353. [[CrossRef](#)]
22. Collivignarelli, M.C.; Abbà, A.; Bertanza, G.; Pedrazzani, R.; Ricciardi, P.; Miino, M.C. Lockdown for CoViD-2019 in Milan: What are the effects on air quality? *Sci. Total Environ.* **2020**, *732*, 139280. [[CrossRef](#)]
23. Hörmann, S.; Jammoul, F.; Kuenzer, T.; Stadlober, E. Separating the impact of gradual lockdown measures on air pollutants from seasonal variability. *Atmos. Pollut. Res.* **2021**, *12*, 84–92. [[CrossRef](#)] [[PubMed](#)]
24. Piccoli, A.; Agresti, V.; Balzarini, A.; Bedogni, M.; Bonanno, R.; Collino, E.; Colzi, F.; Lacavalla, M.; Lanzani, G.; Pirovano, G.; et al. Modeling the Effect of COVID-19 Lockdown on Mobility and NO₂ Concentration in the Lombardy Region. *Atmosphere* **2020**, *11*, 1319. [[CrossRef](#)]
25. Sicard, P.; De Marco, A.; Agathokleous, E.; Feng, Z.; Xu, X.; Paoletti, E.; Rodriguez, J.J.D.; Calatayud, V. Amplified ozone pollution in cities during the COVID-19 lockdown. *Sci. Total Environ.* **2020**, *735*, 139542. [[CrossRef](#)] [[PubMed](#)]
26. Tobias, A.; Carnerero, C.; Reche, C.; Massagué, J.; Via, M.; Minguiñón, M.C.; Alastuey, A.; Querol, X. Changes in air quality during the lockdown in Barcelona (Spain) one month into the SARS-CoV-2 epidemic. *Sci. Total Environ.* **2020**, *726*, 138540. [[CrossRef](#)]
27. Jia, C.; Fu, X.; Bartelli, D.; Smith, L. Insignificant Impact of the “Stay-At-Home” Order on Ambient Air Quality in the Memphis Metropolitan Area, USA. *Atmosphere* **2020**, *11*, 630. [[CrossRef](#)]
28. Zangari, S.; Hill, D.T.; Charette, A.T.; Mirowsky, J.E. Air Quality changes in New York City during the COVID-19 pandemic. *Sci. Total Environ.* **2020**, *742*, 140496. [[CrossRef](#)]
29. Bolaño-Ortiz, T.R.; Pascual-Flores, R.M.; Puliafito, S.E.; Camargo-Cacedo, Y.; Berná-Peña, L.L.; Ruggeri, M.F.; Lopez-Noreña, A.I.; Tames, M.F.; Cereceda-Balic, F. Spread of COVID-19, Meteorological Conditions and Air Quality in the City of Buenos Aires, Argentina: Two Facets Observed during Its Pandemic Lockdown. *Atmosphere* **2020**, *11*, 1045. [[CrossRef](#)]
30. Dantas, G.; Siciliano, B.; França, B.B.; da Silva, C.M.; Arbilla, G. The impact of COVID-19 partial lockdown on the air quality of the city of Rio de Janeiro, Brazil. *Sci. Total Environ.* **2020**, *729*, 139085. [[CrossRef](#)]
31. Bauwens, M.; Compennolle, S.; Stavrakou, T.; Müller, J.-F.; van Gent, J.; Eskes, H.; Levelt, P.F.; van der A, R.; Veeffkind, J.P.; Vlietinck, J.; et al. Impact of coronavirus outbreak on NO₂ pollution assessed using TROPOMI and OMI observations. *Geophys. Res. Lett.* **2020**, *47*, e2020GL087978. [[CrossRef](#)]
32. Dumka, U.C.; Kaskaoutis, D.G.; Verma, S.; Ningombam, S.S.; Kumar, S.; Ghosh, S. Silver linings in the dark clouds of COVID-19: Improvement of air quality over India and Delhi metropolitan area from measurements and WRF-CHIMERE model simulations. *Atmos. Pollut. Res.* **2021**, *12*, 225–242. [[CrossRef](#)]
33. Koukoulis, M.-E.; Skoulidou, I.; Karavias, A.; Parcharidis, I.; Balis, D.; Manders, A.; Segers, A.; Eskes, H.; Van Geffen, J. Sudden changes in nitrogen dioxide emissions over Greece due to lockdown after the outbreak of COVID-19. *Atmos. Chem. Phys. Discuss.* **2020**, 1–17. [[CrossRef](#)]
34. Acharya, P.; Barik, G.; Gayen, B.K.; Bar, S.; Maiti, A.; Sarkar, A.; Ghosh, S.; De, S.K.; Sreelesh, S. Revisiting the levels of Aerosol Optical Depth in South-Southeast Asia, Europe and USA amid the COVID-19 pandemic using satellite observations. *Environ. Res.* **2020**, *193*, 110514. [[CrossRef](#)]
35. Ranjan, A.K.; Patra, A.K.; Gorai, A.K. Effect of lockdown due to SARS COVID-19 on aerosol optical depth (AOD) over urban and mining regions in India. *Sci. Total Environ.* **2020**, *745*, 141024. [[CrossRef](#)]
36. Arregocés, H.A.; Rojano, R.; Restrepo, G. Impact of lockdown on particulate matter concentrations in Colombia during the COVID-19 pandemic. *Sci. Total Environ.* **2020**, *764*, 142874. [[CrossRef](#)] [[PubMed](#)]
37. Zhao, X.P. Impact of COVID-19 Lockdowns and Australian Bushfires on Aerosol Loading over the Downwind Oceanic Regions. *Adv. Environ. Eng. Res.* **2020**, *1*, 19. [[CrossRef](#)]

38. Anil, I.; Alagha, O. Source apportionment of ambient black carbon during the COVID-19 lockdown. *Intern. J. Environ. Res. Public Health* **2020**, *17*, 9021. [[CrossRef](#)]
39. Evangelizou, N.; Platt, S.M.; Eckhardt, S.; Myhre, C.L.; Laj, P.; Arboledas, L.A.; Backman, J.; Brem, B.T.; Fiebig, M.; Flentje, H.; et al. Changes in black carbon emissions over Europe due to COVID-19 lockdowns. *Atmos. Chem. Phys. Discuss.* **2020**, 1–33. [[CrossRef](#)]
40. Grivas, G.; Athanasopoulou, E.; Kakouri, A.; Bailey, J.; Liakakou, E.; Stavroulas, I.; Kalkavouras, P.; Bougiatioti, A.; Kaskaoutis, D.G.; Ramonet, M.; et al. Integrating in situ measurements and city scale modelling to assess the COVID-19 lockdown effects on emissions and air quality in Athens, Greece. *Atmosphere* **2020**, *11*, 1174. [[CrossRef](#)]
41. Wang, H.; Miao, Q.; Shen, L.; Yang, Q.; Wu, Y.; Wei, H.; Yin, Y.; Zhao, T.; Zhu, B.; Lu, W. Characterization of the aerosol chemical composition during the COVID-19 lockdown period in Suzhou in the Yangtze River Delta, China. *J. Environ. Sci.* **2020**, *102*, 110–122. [[CrossRef](#)]
42. Xiang, J.; Austin, E.; Gould, T.; Larson, T.; Shirai, J.; Liu, Y.; Marshall, J.; Seto, E. Impacts of the COVID-19 responses on traffic-related air pollution in a Northwestern US city. *Sci. Total Environ.* **2020**, *747*, 141325. [[CrossRef](#)] [[PubMed](#)]
43. Chen, Y.; Zhang, S.; Peng, C.; Shi, G.; Tian, M.; Huang, R.-J.; Guo, D.; Wang, H.; Yao, X.; Yang, F. Impact of the COVID-19 pandemic and control measures on air quality and aerosol light absorption in Southwestern China. *Sci. Total Environ.* **2020**, *749*, 141419. [[CrossRef](#)]
44. Kalluri, R.O.R.; Gugamsetty, B.; Tandule, C.R.; Kotalo, R.G.; Reddy Thotli, L.; Reddy, R.R.; Palle, S.N.R. Impact of aerosols on surface ozone during COVID-19 pandemic in southern India: A multi-instrumental approach from ground and satellite observations, and model simulations. *J. Atmos. Sol. Terr. Phys.* **2020**, *221*, 105491. [[CrossRef](#)]
45. Collaud Coen, M.; Andrews, E.; Alastuey, A.; Arsov, T.P.; Backman, J.; Brem, B.T.; Bukowiecki, N.; Couret, C.; Eleftheriadis, K.; Flentje, H.; et al. Multidecadal trend analysis of aerosol radiative properties at a global scale. *Atmos. Chem. Phys. Discuss.* **2020**, *14*, 8867–8908. [[CrossRef](#)]
46. Nabat, P.; Somot, S.; Cassou, C.; Mallet, M.; Michou, M.; Bouniol, D.; Decharme, B.; Drugé, T.; Roehrig, R.; Saint-Martin, D. Modulation of radiative aerosols effects by atmospheric circulation over the Euro-Mediterranean region. *Atmos. Chem. Phys. Discuss.* **2020**, *20*, 8315–8349. [[CrossRef](#)]
47. Antón, M.; Valenzuela, A.; Cazorla, A.; Gil, J.E.; Fernández-Gálvez, J.; Lyamani, H.; Foyo-Moreno, I.; Olmo, F.J.; Alados-Arboledas, L. Global and diffuse shortwave irradiance during a strong desert dust episode at Granada (Spain). *Atmos. Res.* **2012**, *118*, 232–239. [[CrossRef](#)]
48. Singh, N.; Banerjee, T.; Raju, M.P.; Deboudt, K.; Sorek-Hamer, M.; Singh, R.S.; Mall, R.K. Aerosol chemistry, transport, and climatic implications during extreme biomass burning emissions over the Indo-Gangetic Plain. *Atmos. Chem. Phys.* **2018**, *18*, 14197–14215. [[CrossRef](#)]
49. Weber, J.; Shin, Y.M.; Staunton Sykes, J.; Archer-Nicholls, S.; Abraham, N.L.; Archibald, A.T. Minimal climate impacts from short-lived climate forcers following emission reductions related to the COVID-19 pandemic. *Geophys. Res. Lett.* **2020**, *47*, e2020GL090326. [[CrossRef](#)]
50. Paraskevopoulou, D.; Liakakou, E.; Gerasopoulos, E.; Mihalopoulos, N. Sources of atmospheric aerosol from long-term measurements (5 years) of chemical composition in Athens, Greece. *Sci. Total Environ.* **2015**, *527–528*, 165–178. [[CrossRef](#)]
51. Diapouli, E.; Manousakas, M.; Vratolis, S.; Vasilatou, V.; Maggos, T.; Saraga, D.; Grigoratos, T.; Argyropoulos, G.; Voutsas, D.; Samara, C.; et al. Evolution of air pollution source contributions over one decade, derived by PM10 and PM2.5 source apportionment in two metropolitan urban areas in Greece. *Atmos. Environ.* **2017**, *164*, 416–430. [[CrossRef](#)]
52. Grivas, G.; Cheristanidis, S.; Chaloulakou, A.; Koutrakis, P.; Mihalopoulos, N. Elemental composition and source apportionment of fine and coarse particles at traffic and urban background locations in Athens, Greece. *Aerosol Air Qual. Res.* **2018**, *18*, 1642–1659. [[CrossRef](#)]
53. Theodosi, C.; Tsagkaraki, M.; Zampas, P.; Grivas, G.; Liakakou, E.; Paraskevopoulou, D.; Lianou, M.; Gerasopoulos, E.; Mihalopoulos, N. Multi-year chemical composition of the fine aerosol fraction in Athens, Greece, with emphasis on the contribution of residential heating in wintertime. *Atmos. Chem. Phys.* **2018**, *18*, 14371–14391. [[CrossRef](#)]
54. Liakakou, E.; Stavroulas, I.; Kaskaoutis, D.G.; Grivas, G.; Paraskevopoulou, D.; Dumka, U.C.; Tsagkaraki, M.; Bougiatioti, A.; Oikonomou, K.; Sciare, J.; et al. Long-term variability, source apportionment and spectral properties of black carbon at an urban background site in Athens, Greece. *Atmos. Environ.* **2020**, *222*, 117137. [[CrossRef](#)]
55. Dumka, U.C.; Tiwari, S.; Kaskaoutis, D.G.; Hopke, P.K.; Singh, J.; Srivastava, A.K.; Bisht, D.S.; Attri, S.D.; Tyagi, S.; Misra, A.; et al. Assessment of PM2.5 chemical compositions in Delhi: Primary vs. secondary emissions and contribution to light extinction coefficient and visibility degradation. *J. Atmos. Chem.* **2017**, *74*, 423–450. [[CrossRef](#)]
56. Katsanos, D.; Bougiatioti, A.; Liakakou, E.; Kaskaoutis, D.G.; Stavroulas, I.; Paraskevopoulou, D.; Lianou, M.; Psiloglou, B.E.; Gerasopoulos, E.; Pilinis, C.; et al. Optical Properties of Near-surface Urban Aerosols and their Chemical Tracing in a Mediterranean City (Athens). *Aerosol Air Qual. Res.* **2019**, *19*, 49–70. [[CrossRef](#)]
57. Demertzis, K.; Tsiotas, D.; Magafas, L. Modeling and forecasting the COVID-19 temporal spread in Greece: An exploratory approach based on complex network defined splines. *Int. J. Environ. Res. Public Health* **2020**, *17*, 4693. [[CrossRef](#)]
58. Grivas, G.; Stavroulas, I.; Liakakou, E.; Kaskaoutis, D.G.; Bougiatioti, A.; Paraskevopoulou, D.; Gerasopoulos, E.; Mihalopoulos, N. Measuring the spatial variability of Black Carbon in Athens during wintertime. *Air Qual. Atmos. Health* **2019**, *12*, 1405–1417. [[CrossRef](#)]

59. Zieger, P.; Väisänen, O.; Corbin, J.C.; Partridge, D.G.; Bastelberger, S.; Mousavi-Fard, M.; Rosati, B.; Gysel, M.; Krieger, U.K.; Leck, C.; et al. Revising the hygroscopicity of inorganic sea salt particles. *Nat. Commun.* **2017**, *8*, 15883. [[CrossRef](#)]
60. Anderson, T.L.; Ogren, J.A. Determining Aerosol Radiative Properties Using the TSI 3563 Integrating Nephelometer. *Aerosol Sci. Technol.* **1998**, *29*, 57–69. [[CrossRef](#)]
61. Pandolfi, M.; Alados-Arboledas, L.; Alastuey, A.; Andrade, M.; Angelov, C.; Artiñano, B.; Backman, J.; Baltensperger, U.; Bonasoni, P.; Bukowiecki, N.; et al. A European aerosol phenomenology-6: Scattering properties of atmospheric aerosol particles from 28 ACTRIS sites. *Atmos. Chem. Phys.* **2018**, *18*, 7877–7911. [[CrossRef](#)]
62. Rajesh, T.A.; Ramachandran, S. Extensive and intensive properties of aerosol over distinct environments: Influence of anthropogenic emissions and meteorology. *J. Atmos. Solar-Terr. Phys.* **2020**, *202*, 105223. [[CrossRef](#)]
63. Schmeisser, L.; Andrews, E.; Ogren, J.A.; Sheridan, P.; Jefferson, A.; Sharma, S.; Kim, J.E.; Sherman, J.P.; Sorribas, M.; Kalapov, I.; et al. Classifying aerosol type using in situ surface spectral aerosol optical properties. *Atmos. Chem. Phys.* **2017**, *17*, 12097–12120. [[CrossRef](#)]
64. Drinovec, L.; Mocnik, G.; Zotter, P.; Prévôt, A.S.H.; Ruckstuhl, C.; Coz, E.; Rupakheti, M.; Sciare, J.; Müller, T.; Wiedensohler, A.; et al. The “dual-spot” Aethalometer: An improved measurement of aerosol black carbon with real time loading compensation. *Atmos. Meas. Tech.* **2015**, *8*, 1965–1979. [[CrossRef](#)]
65. Sandradewi, J.; Prevot, A.S.H.; Weingartner, E.; Schmidhauser, R.; Gysel, M.; Baltensperger, U. A study of wood burning and traffic aerosols in an Alpine valley using a multi-wavelength Aethalometer. *Atmos. Environ.* **2008**, *42*, 101–112. [[CrossRef](#)]
66. Müller, T.; Laborde, M.; Kassell, G.; Wiedensohler, A. Design and performance of a three-wavelength LED-based total scatter and backscatter integrating nephelometer. *Atmos. Meas. Tech.* **2011**, *4*, 1291–1303. [[CrossRef](#)]
67. Sciare, J.; Oikonomou, K.; Cachier, H.; Mihalopoulos, N.; Andreae, M.O.; Maenhaut, W.; Sarda-Estève, R. Aerosol mass closure and reconstruction of the light scattering coefficient over the Eastern Mediterranean Sea during the MINOS campaign. *Atmos. Chem. Phys.* **2005**, *5*, 2253–2265. [[CrossRef](#)]
68. Vrekoussis, M.; Liakakou, E.; Koçak, M.; Kubilay, N.; Oikonomou, K.; Sciare, J.; Mihalopoulos, N. Seasonal variability of optical properties of aerosols in the Eastern Mediterranean. *Atmos. Environ.* **2005**, *39*, 7083–7094. [[CrossRef](#)]
69. Kalivitis, N.; Bougiatioti, A.; Kouvarakis, G.; Mihalopoulos, N. Long term measurements of atmospheric aerosol optical properties in the Eastern Mediterranean. *Atmos. Res.* **2011**, *102*, 351–357. [[CrossRef](#)]
70. Kaskaoutis, D.G.; Grivas, G.; Stavroulas, I.; Liakakou, E.; Dumka, U.C.; Dimitriou, K.; Gerasopoulos, E.; Mihalopoulos, N. In situ identification of aerosol types in Athens, Greece, based on long-term optical and on online chemical characterization. *Atmos. Environ.* **2021**, *246*, 118070. [[CrossRef](#)]
71. Moosmüller, H.; Chakrabarty, R.K.; Ehlers, K.M.; Arnott, W.P. Absorption Ångström coefficient, brown carbon, and aerosols: Basic concepts, bulk matter, and spherical particles. *Atmos. Chem. Phys.* **2011**, *11*, 1217–1225. [[CrossRef](#)]
72. Solomos, S.; Kalivitis, N.; Mihalopoulos, N.; Amiridis, V.; Kouvarakis, G.; Gkikas, A.; Biniotoglou, I.; Tsekeri, A.; Kazadzis, S.; Kottas, M.; et al. From tropospheric folding to khamsin and foehn winds: How atmospheric dynamics advanced a record-breaking dust episode in Crete. *Atmosphere* **2018**, *9*, 240. [[CrossRef](#)]
73. Schuster, G.L.; Dubovik, O.; Arola, A.; Eck, T.F.; Holben, B.N. Remote sensing of soot carbon—Part 2: Understanding the absorption Ångström exponent. *Atmos. Chem. Phys.* **2016**, *16*, 1587–1602. [[CrossRef](#)]
74. Titos, G.; Lyamani, H.; Pandolfi, M.; Alastuey, A.; Alados-Arboledas, L. Identification of fine (PM₁) and coarse (PM₁₀₋₁) sources of particulate matter in an urban environment. *Atmos. Environ.* **2014**, *89*, 593–602. [[CrossRef](#)]
75. Su, T.; Li, Z.; Zheng, Y.; Luan, Q.; Guo, J. Abnormally shallow boundary layer associated with severe air pollution during the COVID-19 lockdown in China. *Geophys. Res. Lett.* **2020**, *47*, e2020GL090041. [[CrossRef](#)]
76. Fourtziou, L.; Liakakou, E.; Stavroulas, I.; Theodosi, C.; Zarbas, P.; Psiloglou, B.; Sciare, J.; Maggos, T.; Bairachtari, K.; Bougiatioti, A.; et al. Multi-tracer approach to characterize domestic wood burning in Athens (Greece) during wintertime. *Atmos. Environ.* **2017**, *148*, 89–101. [[CrossRef](#)]
77. Kaskaoutis, D.G.; Dumka, U.C.; Rashki, A.; Psiloglou, B.E.; Gavriil, A.; Mofidi, A.; Petrinoli, K.; Karagiannis, D.; Kambezidis, H.D. Analysis of intense dust storms over the eastern Mediterranean in March 2018: Impact on radiative forcing and Athens air quality. *Atmos. Environ.* **2019**, *209*, 23–39. [[CrossRef](#)]
78. Paredes-Miranda, G.; Arnott, W.P.; Jimenez, J.L.; Aiken, A.C.; Gaffney, J.S.; Marley, N.A. Primary and secondary contributions to aerosol light scattering and absorption in Mexico City during the MILAGRO 2006 campaign. *Atmos. Chem. Phys.* **2009**, *9*, 3721–3730. [[CrossRef](#)]
79. McMeeking, G.R.; Morgan, W.T.; Flynn, M.; Highwood, E.J.; Turnbull, K.; Haywood, J.; Coe, H. Black carbon aerosol mixing state, organic aerosols and aerosol optical properties over the United Kingdom. *Atmos. Chem. Phys.* **2011**, *11*, 9037–9052. [[CrossRef](#)]
80. Stavroulas, I.; Bougiatioti, A.; Paraskevopoulou, D.; Grivas, G.; Liakakou, E.; Gerasopoulos, E.; Mihalopoulos, N. Sources and processes that control the submicron organic aerosol in an urban Mediterranean environment (Athens) using high temporal resolution chemical composition measurements. *Atmos. Chem. Phys.* **2019**, *19*, 901–919. [[CrossRef](#)]
81. Paraskevopoulou, D.; Liakakou, E.; Gerasopoulos, E.; Theodosi, C.; Mihalopoulos, N. Long-term characterization of organic and elemental carbon in the PM_{2.5} fraction: The case of Athens, Greece. *Atmos. Chem. Phys.* **2014**, *14*, 13313–13325. [[CrossRef](#)]
82. Progiou, A.G.; Ziomas, I.C. Road traffic emissions impact on air quality of the Greater Athens Area based on a 20year emissions inventory. *Sci. Total Environ.* **2011**, *410–411*, 1–7. [[CrossRef](#)]

83. Degraeuwe, B.; Thunis, P.; Clappier, A.; Weiss, M.; Lefebvre, W.; Janssen, S.; Vranckx, S. Impact of passenger car NOX emissions on urban NO2 pollution—Scenario analysis for 8 European cities. *Atmos. Environ.* **2017**, *171*, 330–333. [[CrossRef](#)]
84. Vogiatzis, K.; Zafiropoulou, V.; Gerolymatou, G.; Dimitriou, D.; Halkias, B.; Papadimitriou, A.; Konstantinidis, A. The noise climate at the time of SARS-CoV-2 VIRUS/COVID-19 disease in Athens—Greece: The case of Athens International Airport and the Athens Ring Road (Attiki Odos). *Noise Mapp.* **2020**, *7*, 154–170. [[CrossRef](#)]
85. Gratsea, M.; Liakakou, E.; Mihalopoulos, N.; Adamopoulos, A.; Tsilibari, E.; Gerasopoulos, E. The combined effect of reduced fossil fuel consumption and increasing biomass combustion on Athens' air 713 quality, as inferred from long term CO measurements. *Sci. Total Environ.* **2017**, *592*, 115–123. [[CrossRef](#)]
86. Kalogridis, A.C.; Vratolis, S.; Liakakou, E.; Gerasopoulos, E.; Mihalopoulos, N.; Eleftheriadis, K. Assessment of wood burning versus fossil fuel contribution to wintertime black carbon and carbon monoxide concentrations in Athens, Greece. *Atmos. Chem. Phys.* **2018**, *18*, 10219–10236. [[CrossRef](#)]
87. Hess, M.; Koepke, P.; Schult, I. Optical properties of aerosols and clouds: The software package OPAC. *Bull. Am. Meteorol. Soc.* **1998**, *80*, 831–844. [[CrossRef](#)]
88. Lyamani, H.; Olmo, F.J.; Alados-Arboledas, L. Light scattering and absorption properties of aerosol particles in the urban environment of Granada, Spain. *Atmos. Environ.* **2008**, *42*, 2630–2642. [[CrossRef](#)]
89. Pandolfi, M.; Cusack, M.; Alastuey, A.; Querol, X. Variability of aerosol optical properties in the Western Mediterranean Basin. *Atmos. Chem. Phys.* **2011**, *11*, 8189–8203. [[CrossRef](#)]
90. Titos, G.; Foyo-Moreno, I.; Lyamani, H.; Querol, X.; Alastuey, A.; Alados-Arboledas, L. Optical properties and chemical composition of aerosol particles at an urban location: An estimation of the aerosol mass scattering and absorption efficiencies. *J. Geophys. Res.* **2012**, *117*, D04206. [[CrossRef](#)]
91. Romano, S.; Perrone, M.R.; Pavese, G.; Esposito, F.; Calvello, M. Optical properties of PM2.5 particles: Results from a monitoring campaign in southeastern Italy. *Atmos. Environ.* **2019**, *203*, 35–47. [[CrossRef](#)]
92. Valenzuela, A.; Olmo, F.J.; Lyamani, H.; Antón, M.; Titos, G.; Cazorla, A.; Alados-Arboledas, L. Aerosol scattering and absorption Angström exponents as indicators of dust and dust-free days over Granada (Spain). *Atmos. Res.* **2015**, *154*, 1–13. [[CrossRef](#)]
93. Ealo, M.; Alastuey, A.; Pérez, N.; Ripoll, A.; Querol, X.; Pandolfi, M. Impact of aerosol particle sources on optical properties in urban, regional and remote areas in the north-western Mediterranean. *Atmos. Chem. Phys.* **2018**, *18*, 1149–1169. [[CrossRef](#)]
94. Lack, D.A.; Langridge, J.M. On the attribution of black and brown carbon light absorption using the Ångström exponent. *Atmos. Chem. Phys.* **2013**, *13*, 10535–10543. [[CrossRef](#)]
95. Zotter, P.; Herich, H.; Gysel, M.; El-Haddad, I.; Zhang, Y.; Močnik, G.; Hüglin, C.; Baltensperger, U.; Szidat, S.; Prévôt, A.S.H. Evaluation of the absorption Ångström exponents for traffic and wood burning in the Aethalometer-based source apportionment using radiocarbon measurements of ambient aerosol. *Atmos. Chem. Phys.* **2017**, *17*, 4229–4249. [[CrossRef](#)]
96. Wang, Q.; Liu, H.; Ye, J.; Tian, J.; Zhang, T.; Zhang, Y.; Liu, S.; Cao, J. Estimating Absorption Ångström Exponent of Black Carbon Aerosol by Coupling Multiwavelength Absorption with Chemical Composition. *Environ. Sci. Tech. Lett.* **2020**. [[CrossRef](#)]
97. Li, J.; Carlson, B.E.; Lacis, A.A. Using single-scattering albedo spectral curvature to characterize East Asian aerosol mixtures. *J. Geophys. Res.* **2015**, *120*, 2037–2052. [[CrossRef](#)]
98. Sarkar, C.; Sinha, V.; Sinha, B.; Panday, A.K.; Rupakheti, M.; Lawrence, M.G. Source apportionment of NMVOCs in the Kathmandu Valley during the SusKat-ABC international field campaign using positive matrix factorization. *Atmos. Chem. Phys.* **2017**, *17*, 8129–8156. [[CrossRef](#)]
99. Liakakou, E.; Kaskaoutis, D.G.; Grivas, G.; Stavroulas, I.; Tsagkaraki, M.; Paraskevopoulou, D.; Bougiatioti, A.; Dumka, U.C.; Gerasopoulos, E.; Mihalopoulos, N. Long-term brown carbon spectral characteristics in a Mediterranean city (Athens). *Sci. Total Environ.* **2020**, *708*, 135019. [[CrossRef](#)] [[PubMed](#)]
100. Romano, S.; Vecchi, R.; Perrone, M.R. Intensive optical parameters of pollution sources identified by positive matrix factorization technique. *Atmos. Res.* **2020**, *244*, 105029. [[CrossRef](#)]
101. Zhang, X.; Mao, M.; Chen, H.; Tang, S. Theoretical study of scattering Angstrom exponent of coated black carbon aerosols: The effect of microphysical configurations. *J. Quant. Spectrosc. Radiat. Transf.* **2020**, *256*, 107302. [[CrossRef](#)]
102. Grivas, G.; Cheristanidis, S.; Chaloulakou, A. Elemental and organic carbon in the urban environment of Athens. Seasonal and diurnal variations and estimates of secondary organic carbon. *Sci. Total Environ.* **2012**, *414*, 535–545. [[CrossRef](#)] [[PubMed](#)]
103. Kaskaoutis, D.G.; Grivas, G.; Theodosi, C.; Tsagkaraki, M.; Paraskevopoulou, D.; Stavroulas, I.; Liakakou, E.; Gkikas, A.; Hatzianastassiou, N.; Wu, C.; et al. Carbonaceous aerosols in contrasting atmospheric environments in Greek cities: Evaluation of the EC-tracer methods for secondary organic carbon estimation. *Atmosphere* **2020**, *11*, 161. [[CrossRef](#)]
104. Ram, K.; Sarin, M.; Hegde, P. Long-term record of aerosol optical properties and chemical composition from a high-altitude site (Manora Peak) in Central Himalaya. *Atmos. Chem. Phys.* **2010**, *10*, 11791–11803. [[CrossRef](#)]
105. Costabile, F.; Alas, H.; Aufderheide, M.; Avino, P.; Amato, F.; Argentini, S.; Barnaba, F.; Berico, M.; Bernardoni, V.; Biondi, R.; et al. First results of the “Carbonaceous Aerosol in Rome and Environs (CARE)” Experiment: Beyond Current Standards for PM10. *Atmosphere* **2017**, *8*, 249. [[CrossRef](#)]
106. Chatterjee, A.; Mukherjee, S.; Dutta, M.; Ghosh, A.; Ghosh, S.K.; Roy, A. High rise in carbonaceous aerosols under very low anthropogenic emissions over eastern Himalaya, India: Impact of lockdown for COVID-19 outbreak. *Atmos. Environ.* **2020**, *244*, 117947. [[CrossRef](#)]

107. Dubovik, O.; Holben, B.N.; Eck, T.F.; Smirnov, A.; Kaufman, Y.J.; King, M.D.; Tanrè, D.; Slutsker, I. Variability of absorption and optical properties of key aerosol types observed in worldwide locations. *J. Atmos. Sci.* **2002**, *59*, 590–608. [[CrossRef](#)]
108. Stockwell, C.E.; Christian, T.J.; Goetz, J.D.; Jayarathne, T.; Bhawe, P.V.; Praveen, P.S.; Adhikari, S.; Maharjan, R.; DeCarlo, P.F.; Stone, E.A.; et al. Nepal Ambient Monitoring and Source Testing Experiment (NAMASTE): Emissions of trace gases and light-absorbing carbon from wood and dung cooking fires, garbage and crop residue burning, brick kilns, and other sources. *Atmos. Chem. Phys.* **2016**, *16*, 11043–11081. [[CrossRef](#)]
109. Izhar, S.; Gupta, T.; Panday, A.K. Improved method to apportion optical absorption by black and brown carbon under the influence of haze and fog at Lumbini, Nepal, on the Indo-Gangetic Plains. *Environ. Pollut.* **2020**, *263*, 114640. [[CrossRef](#)]
110. Pandey, A.; Hsu, A.; Tiwari, S.; Pervez, S.; Chakrabarty, R.K. Light Absorption by Organic Aerosol Emissions Rivals That of Black Carbon from Residential Biomass Fuels in South Asia. *Environ. Sci. Technol. Lett.* **2020**, *7*, 266–272. [[CrossRef](#)]
111. Yuan, W.; Huang, R.-J.; Yang, L.; Guo, J.; Chen, Z.; Duan, J.; Wang, T.; Ni, H.; Han, Y.; Li, Y.; et al. Characterization of the light-absorbing properties, chromosphere composition and sources of brown carbon aerosol in Xi'an, northwestern China. *Atmos. Chem. Phys.* **2020**, *20*, 5129–5144. [[CrossRef](#)]
112. Zhang, Y.; Albinet, A.; Petit, J.-E.; Jacob, V.; Chevrier, F.; Gille, G.; Pontet, S.; Chrétien, E.; Dominik-Sègue, M.; Levigoureux, G.; et al. Substantial brown carbon emissions from wintertime residential wood burning over France. *Sci. Total Environ.* **2020**, *743*, 140752. [[CrossRef](#)]
113. Derimian, Y.; Karnieli, A.; Kaufman, Y.J.; Andreae, M.O.; Andreae, T.W.; Dubovik, O.; Maenhaut, W.; Koren, I. The role of iron and black carbon in aerosol light absorption. *Atmos. Chem. Phys.* **2008**, *8*, 3623–3637. [[CrossRef](#)]
114. Patel, P.N.; Dumka, U.C.; Kaskaoutis, D.G.; Babu, K.N.; Mathur, A.K. Optical and radiative properties of aerosols over Desalpar, a remote site in western India: Source identification, modification processes and aerosol type discrimination. *Sci. Total Environ.* **2017**, *575*, 612–627. [[CrossRef](#)]
115. Raptis, I.-P.; Kazadzis, S.; Eleftheratos, K.; Amiridis, V.; Fountoulakis, I. Single Scattering Albedo's spectral dependence effect on UV irradiance. *Atmosphere* **2018**, *9*, 364. [[CrossRef](#)]
116. Russell, P.B.; Bergstrom, R.W.; Shinozuka, Y.; Clarke, A.D.; De-Carlo, P.F.; Jimenez, J.L.; Livingston, J.M.; Redemann, J.; Dubovik, O.; Strawa, A. Absorption Angstrom Exponent in AERONET and related data as an indicator of aerosol composition. *Atmos. Chem. Phys.* **2010**, *10*, 1155–1169. [[CrossRef](#)]
117. Habib, G.; Venkataraman, C.; Bond, T.C.; Schauer, J.J. Chemical, microphysical and optical properties of primary particles from the combustion of biomass fuels. *Environ. Sci. Technol.* **2008**, *42*, 8829–8834. [[CrossRef](#)] [[PubMed](#)]
118. Valentini, S.; Barnaba, F.; Bernardoni, V.; Calzola, G.; Costabile, F.; Di Liberto, L.; Forello, A.C.; Gobbi, G.P.; Gualtieri, M.; Lucarelli, F.; et al. Classifying aerosol particles through the combination of optical and physical-chemical properties: Results from a wintertime campaign in Rome (Italy). *Atmos. Res.* **2020**, *235*, 104799. [[CrossRef](#)]
119. Zhang, K.M.; Allen, G.; Yang, B.; Chen, G.; Gu, J.; Schwab, J.; Felton, D.; Rattigan, O. Joint measurements of PM_{2.5} and light-absorptive PM in wood smoke dominated ambient and plume environments. *Atmos. Chem. Phys.* **2017**, *17*, 11441–11452. [[CrossRef](#)]
120. Li, S.; Zhu, M.; Yang, W.; Tang, M.; Huang, X.; Yu, Y.; Fang, H.; Yu, X.; Yu, Q.; Fu, X.; et al. Filter-based measurement of light absorption by brown carbon in PM_{2.5} in a megacity in South China. *Sci. Total Environ.* **2018**, *633*, 1360–1369. [[CrossRef](#)]
121. Costabile, F.; Barnaba, F.; Angelini, F.; Gobbi, G.P. Identification of key aerosol populations through their size and composition resolved spectral scattering and absorption. *Atmos. Chem. Phys.* **2013**, *13*, 2455–2470. [[CrossRef](#)]
122. Liu, D.; Allan, J.D.; Young, D.E.; Coe, H.; Beddows, D.; Fleming, Z.L.; Flynn, M.J.; Gallagher, M.W.; Harrison, R.M.; Lee, J.; et al. Size distribution, mixing state and source apportionment of black carbon aerosol in London during wintertime. *Atmos. Chem. Phys.* **2014**, *14*, 10061–10084. [[CrossRef](#)]
123. Zhang, X.; Mao, M.; Chen, H.; Tang, S. The single scattering albedo Angstrom exponent of black carbon with brown coatings. *J. Quant. Spectrosc. Radiat. Transf.* **2021**, *259*, 107429. [[CrossRef](#)]
124. Kaskaoutis, D.G.; Kambezidis, H.D.; Hatzianastassiou, N.; Kosmopoulos, P.G.; Badarinath, K.V.S. Aerosol Climatology: Dependence of the Ångström exponent on wavelength over four AERONET sites. *Atmos. Chem. Phys. Discuss.* **2007**, *7*, 7347–7397.
125. Boselli, A.; Caggiano, R.; Cornacchia, C.; Madonna, F.; Mona, L.; Macchiato, M.; Pappalardo, G.; Trippetta, S. Multi year sun-photometer measurements for aerosol characterization in a Central Mediterranean site. *J. Atmos. Res.* **2012**, *104–105*, 98–110. [[CrossRef](#)]
126. Raptis, I.-P.; Kazadzis, S.; Amiridis, V.; Gkikas, A.; Gerasopoulos, E.; Mihalopoulos, N. Decade of Aerosol Optical Properties Measurements over Athens, Greece. *Atmosphere* **2020**, *11*, 154. [[CrossRef](#)]
127. Lack, D.A.; Cappa, C.D. Impact of brown and clear carbon on light absorption enhancement, single scatter albedo and absorption wavelength dependence of black carbon. *Atmos. Chem. Phys.* **2010**, *10*, 4207–4220. [[CrossRef](#)]
128. Saleh, R.; Marks, M.; Heo, J.; Adams, P.J.; Donahue, N.M.; Robinson, A.L. Contribution of brown carbon and lensing to the direct radiative effect of carbonaceous aerosols from biomass and biofuel burning emissions. *J. Geophys. Res.* **2015**, *120*, 10285–10296. [[CrossRef](#)]
129. Shamjad, P.M.; Satish, R.V.; Thamban, N.M.; Rastogi, N.; Tripathi, S.N. Absorbing Refractive Index and Direct Radiative Forcing of Atmospheric Brown Carbon over Gangetic Plain. *ACS Earth Space Chem.* **2018**, *2*, 31–37. [[CrossRef](#)]

130. Cazorla, A.; Bahadur, R.; Suski, K.J.; Cahill, J.F.; Chand, D.; Schmid, B.; Ramanathan, V.; Prather, K.A. Relating aerosol absorption due to soot, organic carbon, and dust to emission sources determined from in-situ chemical measurements. *Atmos. Chem. Phys.* **2013**, *13*, 9337–9350. [[CrossRef](#)]
131. Cappa, C.D.; Kolesar, K.R.; Zhang, X.; Atkinson, D.B.; Pekour, M.S.; Zaveri, R.A.; Zelenyuk, A.; Zhang, Q. Understanding the optical properties of ambient sub and supermicron particulate matter: Results from the CARES 2010 field study in northern California. *Atmos. Chem. Phys.* **2016**, *16*, 6511–6535. [[CrossRef](#)]
132. Rupakheti, D.; Kang, S.; Rupakheti, M.; Cong, Z.; Panday, A.K.; Holben, B.N. Identification of absorbing aerosol types at a site in the northern edge of Indo-Gangetic Plain and a polluted valley in the foothills of the central Himalayas. *Atmos. Res.* **2019**, *223*, 15–23. [[CrossRef](#)]
133. Kumar, K.R.; Boiyo, R.; Khan, R.; Kang, N.; Yu, X.; Sivakumar, V.; Griffith, D.; Devi, N.L. Multi-year analysis of aerosol optical properties and implications to radiative forcing over urban Pretoria, South Africa. *Theor. Appl. Climatol.* **2020**, *141*, 343–357. [[CrossRef](#)]
134. Dumka, U.C.; Kaskaoutis, D.G.; Mihalopoulos, N.; Sheoran, R. Identification of key aerosol types and mixing states in the central Indian Himalayas during the GVAX campaign: The role of particle size in aerosol classification. *Sci. Total Environ.* **2020**, *761*, 143188. [[CrossRef](#)] [[PubMed](#)]
135. Wang, Q.; Li, L.; Zhou, J.; Ye, J.; Dai, W.; Liu, H.; Zhang, Y.; Zhang, R.; Tian, J.; Chen, Y.; et al. Measurement report: Source and mixing state of black carbon aerosol in the North China Plain: Implications for radiative effect. *Atmos. Chem. Phys.* **2020**, *20*, 15427–15442. [[CrossRef](#)]